Journal of
Composites Science

MDPI

Article

Extending a Calibrated Average Strain Energy Density (ASED) Criterion for Fracture Load Prediction in Notched 3D-Printed PEEK and Its Fiber-Reinforced Composites

Sergio Arrieta * and Sergio Cicero

Laboratorio de la División de Ciencia e Ingeniería de los Materiales (LADICIM), Departamento de Ciencia e Ingeniería del Terreno y de los Materiales, Universidad de Cantabria, Av. Los Castros, 44, 39005 Santander, Spain; ciceros@unican.es

* Correspondence: sergio.arrieta@unican.es

Abstract

This study evaluates a calibrated Average Strain Energy Density (ASED) criterion for predicting fracture loads in additively manufactured PEEK and reinforced PEEK composites. Although the ASED criterion is a robust tool for linear-elastic materials, PEEK specimens produced via fused filament fabrication (FFF) exhibit a non-linear behavior that requires a modified approach. This work proposes a calibration of the ASED parameters (the critical strain energy and the control volume radius) to extend the applicability of this criterion to high-performance polymers with non-linear elastic response. The methodology was validated using neat PEEK and reinforced PEEK filaments: carbon-fiber reinforced (10 wt.% and 20 wt.%) and glass-fiber reinforced (20 wt.%). Experimental testing involved single-edge-notched bending (SENB) specimens with varying raster orientations (0/90, 30/−60, and 45/−45) and U-notch radii (0.00 mm—crack-like—0.25 mm, 0.50 mm, 1.00 mm, and 2.00 mm). By correlating the local strain energy distribution at the notch root with the global failure response, the results demonstrate that the calibrated ASED criterion provides highly accurate fracture load predictions across all tested materials. This research offers a reliable structural integrity assessment tool for 3D-printed PEEK components, accounting for the complex interaction between material non-linearity and notch effect, extending previous works on additive manufacturing ABS, PLA, and ASA polymers.

Keywords: additive manufacturing; fused filament fabrication (FFF); polyether-ether-ketone (PEEK); carbon-fiber reinforcement; glass-fiber reinforcement; notch effect; fracture; strain energy density; finite element analysis (FEA)

Check for updates

Academic Editor: Yang Li

Received: 22 October 2026
Revised: 16 November 2026
Accepted: 19 November 2026
Published: 20 November 2026

Copyright: © 2026 by the authors. Licensee MDPI, Basel, Switzerland. This article is an open access article distributed under the terms and conditions of the Creative Commons Attribution (CC BY) license.

1. Introduction

Additive manufacturing (AM) has revolutionized the production of complex geometries across various industries, enabling the fabrication of high-performance components from materials ranging from metals to advanced thermoplastic composites [1]. Among these technologies, material extrusion (MEX), commonly implemented through fused filament fabrication (FFF), has emerged as a prominent method for industrial applications due to its cost-efficiency and design freedom. FFF involves the selective deposition of molten thermoplastic filaments, layer-by-layer, to form a three-dimensional structure [2]. Despite its versatility, the inherent layer-wise morphology and processing-induced defects often result in anisotropic mechanical properties and localized stress concentrations, presenting significant challenges for structural integrity assessment under complex loading conditions.

In fiber-reinforced polymers, these challenges are compounded by FFF-specific defects, such as inter-layer voids, delamination, and surface roughness, alongside poor fiber-matrix interfacial bonding and intra-layer porosity [3].

Polyether-ether-ketone (PEEK) is a semi-crystalline thermoplastic characterized by exceptional thermal stability, high chemical resistance, and a favorable strength-to-weight ratio, making it an ideal candidate for structural applications [4]. Owing to these superior characteristics, 3D-printed PEEK has seen widespread adoption across critical industrial sectors, including aerospace [5], automotive [6], energy [7], and biomedical engineering [8]. Within the medical field, PEEK is particularly valued for its versatility: it is utilized in its neat form [9,10] or combined with various reinforcements to enhance its mechanical properties [11,12], promote bioactivity [13,14], or achieve a synergistic balance of both [15]. The integration of PEEK-based components into these demanding sectors is primarily driven by the urgent industrial requirement for materials capable of maintaining structural integrity and functional reliability under extreme environmental conditions.

Notwithstanding its advantages, when processed via FFF, the mechanical performance of PEEK is significantly influenced by its degree of crystallinity and the quality of the inter-filamentous bonding, both of which are highly dependent on process parameters such as nozzle, chamber, and bed temperatures, or layer thickness [4,16,17]. To enhance the mechanical performance of FFF-printed components, recent research has pivoted toward the development of fiber-reinforced polymer composites [18]. The integration of carbon fibers (CF) and glass fibers (GF) into a PEEK matrix contributes to improving both ultimate tensile strength and Young's modulus [19–23]. Additionally, these mechanical reinforcements can contribute to improving the bioactivity of PEEK [24,25]. However, the mechanical response of these composites is inherently anisotropic, governed primarily by the raster orientation [26–29] and crystallinity degree [30,31].

Despite extensive documentation dealing with the quasi-static tensile properties of FFF-printed PEEK [9,26,32–35] and its short fiber-reinforced composites [21,23,31,36–43], there remains a notable lack of systematic investigation into the fracture behavior [44] of these materials when subjected to notch-like or crack-like defects [45–47]. Given the susceptibility of additively manufactured parts to internal discontinuities, characterizing the fracture resistance of these composites is essential for establishing reliable safety margins and ensuring the structural integrity of critical components in demanding applications. Furthermore, while the addition of fibers, such as carbon or glass, enhances the stiffness and strength of the polymer matrix, it concurrently increases the notch sensitivity of the material and modifies its fracture behavior [48]. Consequently, traditional fracture mechanics approaches, often calibrated for monolithic polymers, frequently struggle to capture the complex fracture initiation and propagation modes observed in FFF-printed PEEK and its composites, necessitating a more robust, energy-based failure criterion.

The complex geometries inherent to additively manufactured components often contain stress risers originating from manufacturing defects, such as surface roughness and interlayer porosity, as well as intentional design features like grooves, holes, and corners. Assessing the structural integrity of these parts requires analytical approaches that extend beyond conventional Linear Elastic Fracture Mechanics (LEFM), which is primarily restricted to sharp, crack-like defects. It has been widely demonstrated [49,50] that non-sharp stress risers, or notches, induce an apparent fracture toughness that typically exceeds the intrinsic toughness measured in cracked specimens. To effectively account for this notch effect, researchers have increasingly turned to volume-based methods, such as the Theory of Critical Distances (TCD) [51] and the Average Strain Energy Density (ASED) criterion [50]. Unlike point-stress criteria [52] that are very sensitive to local manufacturing fluctuations,

the ASED criterion evaluates the energy over a control volume, providing a more stable and representative failure prediction for heterogeneous materials.

While the ASED criterion has been extensively validated across various brittle and quasi-brittle materials [50,53–56], its application to 3D-printed polymers is still an evolving field [57–66]. Most existing studies focus on materials with near-linear elastic responses; however, there remains a critical gap in extending these energy-based models to high-performance polymers like PEEK [67] and its fiber-reinforced variants, which exhibit non-linear fracture behavior due to their semi-crystalline nature and manufacturing-induced anisotropy. This study addresses this gap by evaluating a simplified calibration technique to estimate fracture loads, bypassing the need for complex, computationally intensive simulations. The calibration allows the linear-elastic formulation of the ASED criterion to be used, accounting for the non-linearities through the determination of the material ASED parameters. Although this calibration approach has successfully estimated fracture loads in structural steels [55], polymeric plates [60,63,65,68], and matrix-reinforced polymers [69,70], this work evaluates its predictive capacity for high-performance FFF-printed PEEK and its carbon- or glass-fiber reinforced composites. Using a comprehensive set of 240 single-edge notched bending (SENB) specimens per material, varying in raster orientation and notch radius, we compare standard linear-elastic ASED formulations against a calibrated model that accounts for non-linear phenomena. By correlating the local strain energy distribution with global failure, this research demonstrates the accuracy of the proposed methodology in predicting fracture loads for complex, additively manufactured structural components. Previous works allowed the authors to demonstrate the applicability of the ASED criterion in a number of standard, mechanically conventional FFF polymers and polymer-matrix composites [59,60,68,70]. The present study assesses its applicability to high-performance semi-crystalline PEEK and its fiber composites, where non-linearity, crystallinity, and reinforcement effects are expected to be more significant.

The paper is structured as follows: Section 2 details the filament properties, the FFF fabrication parameters, and the comprehensive experimental and numerical procedures employed for the SENB testing. Section 3 presents the ASED-based fracture load predictions, contrasting the calibrated energy-based model with standard linear-elastic formulations and experimental data. Finally, Section 4 summarize the main findings, emphasizing the versatility and reliability of the calibrated ASED criterion for the structural integrity assessment of FFF-printed PEEK and PEEK composites.

2. Materials and Methods

The materials utilized in this study consist of neat PEEK, carbon-fiber reinforced PEEK (10 wt.% and 20 wt.%), denoted as PEEK-CF10 and PEEK-CF20, and glass-fiber reinforced PEEK (20 wt.%), denoted as PEEK-GF20. These three distinct composites are commercially available from Filoalfa (Ozzero, Italy). All specimens were fabricated using an industrial-grade FFF system in a flat-print orientation. Printing parameters are summarized in Table 1. To ensure high inter-layer adhesion, consistent crystallinity, and smooth material flow, the printing parameters were adapted to each PEEK configuration. In particular, for the PEEK-CF20 composite, a larger nozzle diameter and layer thickness were required due to its higher melt viscosity, preventing fiber agglomeration and nozzle clogging while ensuring defect-free filament deposition.

The specimens were designed according to the SENB configuration. All specimens were printed with 100% infill. The printing parameters were kept constant within each specific material configuration to isolate the effects of raster orientation and fiber content. Three raster orientations (RO) were investigated: 0/90, 30/−60, and 45/−45. Figure 1

shows an example of a complete SENB specimen for each material, illustrating the external appearance and visual quality of the specimens.

Table 1. FFF printing conditions for pure PEEK and its fiber-reinforced composites.

	PEEK	PEEK-CF10	PEEK-CF20	PEEK-GF20
Nozzle diameter (mm)	0.60	0.60	0.80	0.60
Layer thickness (mm)	0.30	0.30	0.34	0.30
Line width (mm)	0.60	0.60	0.80	0.60
Nozzle temperature (°C)	430	440	440	440
Platform temperature (°C)	120	120	120	120
Chamber temperature (°C)	90	90	90	90
Printing speed (mm/s)	45	45	40	40

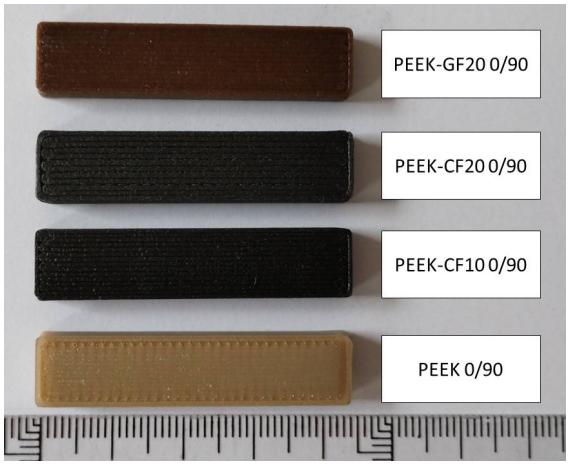

Figure 1. FFF-printed SENB specimens made of PEEK and its composites (PEEK-CF10, PEEK-CF20, and PEEK-GF20) with a 0/90 raster orientation and 100% infill.

A comprehensive experimental campaign was conducted, comprising a total of 276 tests: 36 tensile tests and 240 fracture tests performed on SENB specimens for each material. To investigate the notch effect, the SENB specimens were prepared with five distinct notch radii (ρ): 0.00 mm (representing crack-like defects), 0.25 mm, 0.50 mm, 1.00 mm, and 2.00 mm. Figure 2 provides a schematic illustrating the specimen geometry, dimensions, and the three raster orientations employed. Fracture tests were performed using a Zwick-Roell universal electromechanical testing machine equipped with a 2.5 kN load cell (ZwickRoell, Ulm, Germany). All tests were conducted under displacement control at a constant rate of 1 mm/min to ensure quasi-static loading conditions.

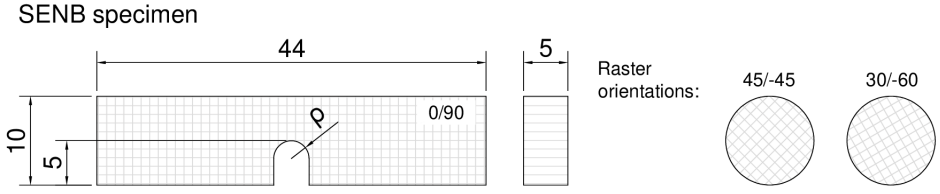

Figure 2. Geometry and dimensions (in mm) of the SENB specimens used in this study, including the investigated raster orientations (0/90, 30/−60, and 45/−45).

In this study, tensile tests were conducted in accordance with ASTM D638 [71], while fracture testing of both cracked and notched specimens followed the procedures outlined in ASTM D5045 [72]. The key mechanical properties derived from these tests are sum-

marized in Table 2 [73]. As illustrated in Figure 3, the stress-strain curves demonstrate that the carbon-fiber reinforced composites (PEEK-CF10 and PEEK-CF20) exhibit significantly higher stiffness compared to neat PEEK, whereas the PEEK-GF20 composite displays intermediate mechanical behavior.

Table 2. Summary of mechanical properties for the FFF-printed composites. E: Young's modulus; σ_y: yield stress; σ_u: ultimate tensile strength; ε_u: strain under maximum load; K_{mat}: fracture toughness.

Material	RO	E (MPa)	σ_y (MPa)	σ_u (MPa)	ε_u (%)	K_{mat} (MPam$^{1/2}$)
PEEK	0/90	2973 ± 309	42.98 ± 6.21	63.16 ± 1.06	3.82 ± 0.02	4.54 ± 0.51
	30/−60	2361 ± 57	48.73 ± 0.21	61.33 ± 1.30	4.27 ± 0.15	4.19 ± 0.64
	45/−45	2601 ± 193	47.08 ± 0.65	59.57 ± 0.72	4.27 ± 0.20	4.60 ± 1.45
PEEK-CF10	0/90	4854 ± 1280	51.29 ± 3.59	59.38 ± 3.95	2.30 ± 0.36	3.07 ± 0.62
	30/−60	4123 ± 778	42.10 ± 2.51	51.87 ± 1.86	2.73 ± 0.55	3.17 ± 0.82
	45/−45	3342 ± 579	35.33 ± 2.55	46.12 ± 3.08	4.59 ± 0.31	2.94 ± 0.38
PEEK-CF20	0/90	7505 ± 1486	65.94 ± 2.30	77.71 ± 0.80	2.47 ± 0.19	4.99 ± 1.18
	30/−60	3418 ± 1190	27.61 ± 2.31	31.95 ± 0.87	1.79 ± 0.93	2.92 ± 0.44
	45/−45	5953 ± 434	51.35 ± 0.66	65.36 ± 1.25	2.56 ± 0.30	4.60 ± 0.98
PEEK-GF20	0/90	4792 ± 1199	55.44 ± 4.28	63.77 ± 3.71	1.97 ± 0.20	3.90 ± 0.66
	30/−60	3477 ± 762	34.68 ± 2.95	40.36 ± 2.50	1.90 ± 0.35	3.52 ± 0.20
	45/−45	2833 ± 151	29.99 ± 1.90	34.42 ± 2.10	2.00 ± 0.09	3.42 ± 0.41

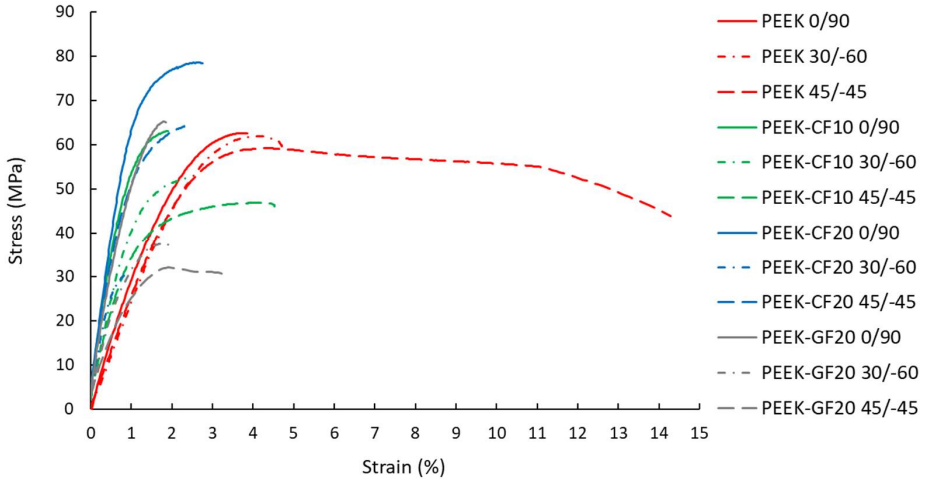

Figure 3. Representative engineering stress-strain curves obtained from tensile tests for neat PEEK, PEEK-CF10, PEEK-CF20, and PEEK-GF20 specimens, illustrating the non-linear response of the tested material.

Following the characterization of fundamental mechanical properties through tensile and fracture testing [73], the failure loads of the U-notched specimens were estimated using the ASED criterion. Initially, a linear-elastic formulation was applied to establish a baseline for fracture load prediction. This standard approach served as a reference point to evaluate the efficacy of the subsequent analysis, which incorporates the inherent non-linearity of the materials and quasi-brittle behavior to refine the fracture load estimations.

The ASED criterion, rooted in the "core region" concept originally proposed by Sih [74] and further refined by Lazzarin and Zambardi [75,76], is a robust framework for predicting fracture initiation. The ASED approach posits that failure in brittle or quasi-brittle materials

occurs when the mean elastic strain energy density (W) within a defined control volume attains a critical value (W_C). For an ideally brittle material, the critical energy density is derived from the fracture toughness (K_{mat}) and the ultimate tensile strength (σ_u) as follows [75]:

$$W_C = \frac{{\sigma_u}^2}{2E} \quad (1)$$

where σ_u is the ultimate tensile strength and E is the Young's modulus.

The ASED criterion requires averaging the strain energy density over a control volume circumscribing the notch root. For two-dimensional plane problems, this volume is represented by a circle or circular sector with a characteristic radius, R_C. For U-notches (where the notch opening angle $2\alpha = 0$), R_C is determined using K_{mat}, σ_u, and Poisson's ratio (ν) [77]:

$$R_C = \frac{(1+\nu)(5-8\nu)}{4\pi}\left(\frac{K_{mat}}{\sigma_u}\right)^2 \text{ plane strain,} \quad (2)$$

$$R_C = \frac{(5-3\nu)}{4\pi}\left(\frac{K_{mat}}{\sigma_u}\right)^2 \text{ plane stress,} \quad (3)$$

The transition between plane strain and plane stress conditions is governed by the specimen thickness (B) and yield strength (σ_y), as defined by the limits in Equation (4) and Equation (5) [51]:

$$K_{mat} < \sigma_y \cdot \left(\frac{B}{2.5}\right)^{1/2} \text{ plane strain,} \quad (4)$$

$$K_{mat} > \sigma_y \cdot (\pi B)^{1/2} \text{ plane stress,} \quad (5)$$

For blunt notches, the total strain energy is quantified within the notch-tip zone (Figure 4), which characterizes the stress field distribution ahead of the geometric discontinuity. Within this region, the ASED is formulated as a function of the maximum elastic notch stress (σ_{max}) [78]. The total strain energy over this specific volume (Ω) is then averaged to determine the ASED, as detailed in Equation (6) [50]:

$$\overline{W} = F(2\alpha)H\left(2\alpha, \frac{R_C}{\rho}\right)\frac{{\sigma_{max}}^2}{E} \quad (6)$$

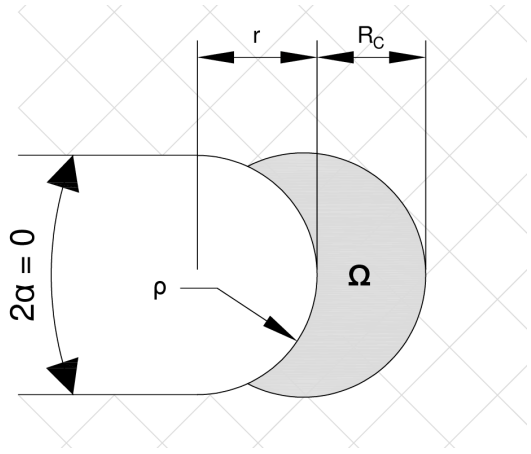

Figure 4. Control volume (Ω) at the notch root for a U-notch under Mode I loading, indicating the region utilized for the ASED.

The parameter $F(2\alpha)$ depends on the notch opening angle; for U-notches, where the opening angle $2\alpha = 0$, this value is 0.785. The function H, which accounts for both the notch geometry (opening angle 2α and notch radius ρ) and the characteristic length of the material,

the critical radius, is essential for computing the average strain energy density. Here, σ_{max} denotes the maximum elastic stress at the notch root. Table 3 provides a comprehensive compilation of H function values for U-shaped notches, as reported in the literature [79]. For a material Poisson's ratio of 0.43 [45,80], the corresponding H values were determined by applying a second-order polynomial extrapolation to the data provided in [79]. This approach ensures a more accurate estimation of H by accounting for the non-linear trend of the material properties across the range of the available dataset.

Table 3. Tabulated H values for U-shaped notches [79]. H values for $\nu = 0.43$ via second-order polynomial extrapolation (italicized column).

2α (rad)	R_C/ρ	$\nu = 0.30$	$\nu = 0.35$	$\nu = 0.40$	$\nu = 0.43$
0	0.01	0.5638	0.5432	0.5194	*0.5036*
0	0.05	0.5086	0.4884	0.4652	*0.4498*
0	0.10	0.4518	0.4322	0.4099	*0.3952*
0	0.30	0.3069	0.2902	0.2713	*0.2589*
0	0.50	0.2276	0.2135	0.1976	*0.1872*
0	1.00	0.1314	0.1217	0.1110	*0.1041*

The fracture behavior and the corresponding critical loads of the U-notched specimens are investigated using the ASED criterion. The failure condition is defined by the equality between the averaged strain energy density within the notch-tip zone and the critical strain energy density of the material:

$$\overline{W} = W_C \tag{7}$$

This criterion serves as the governing condition to predict the fracture initiation load for the various material configurations and notch radii examined in this study. The critical energy value, W_C, is derived by calculating the total area under the experimental tensile stress-strain curves, rather than relying on the simplified linear approximation presented in Equation (1). By equating the averaged strain energy density (Equation (6)) to the critical value (Equation (7)), the following relationship is established to predict the failure load:

$$\sigma_{max-ASED} = \sqrt{\frac{W_C \cdot E}{0.785 \cdot H\left(2\alpha = 0, \frac{R_C}{\rho}\right)}} \tag{8}$$

The derivation of the H-function necessitates a precise definition of the material critical radius, R_C. This parameter is determined by assessing the stress state, choosing between the methodologies represented by Equation (2) and Equation (3). Given the specimen dimensions and material properties examined in this study, the fracture behavior is governed by an intermediate state between plane strain and plane stress conditions; consequently, R_C values are calculated by using linear interpolation between Equations (2) and (3). In several cases during the analysis, the ratio of the critical radius to the notch radius (R_C/ρ) was found to exceed unity. This necessitated the extrapolation of the H values (tabulated in Table 3) by applying the fitting function illustrated in Figure 5. This extrapolation procedure was essential to ensure the accuracy and consistency of the fracture load predictions across all investigated notch radii.

However, as shown in Figure 3 and demonstrated by previous studies [20,26,31,38,40], the materials under investigation exhibit a pronounced non-linear tensile behavior across the three distinct raster orientations. This observed non-linearity suggests that the assumption of a purely linear-elastic response may not fully capture the material's mechanical behavior. Nevertheless, previous research [57,59,60,62,65,66,68–70] has validated alternative approaches for applying the ASED criterion to AM polymers when the extent of this non-linearity remains limited.

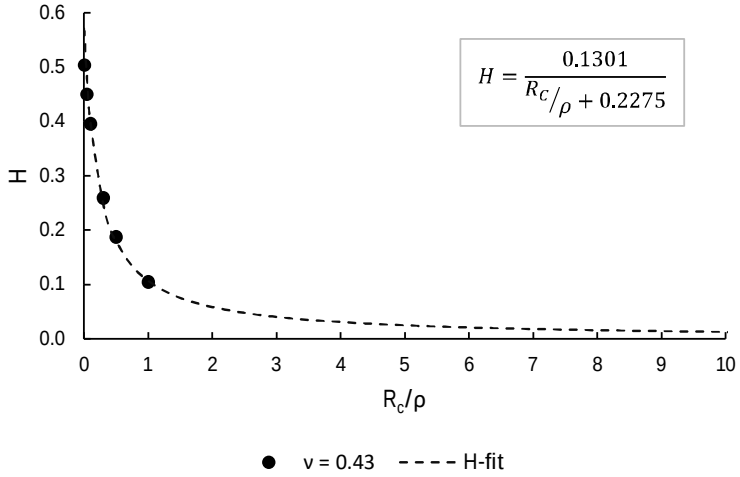

Figure 5. Extrapolation curve for the H-function applied to cases where $R_C/\rho > 1$.

In any case, once $\sigma_{max\text{-}ASED}$ (Equation (8)) is known, the corresponding external load was determined using numerical simulations. Specifically, the stress field within the mid-plane of the fracture section was analyzed for all specimen geometries using a finite element (FE) model developed using Ansys (2023 R1 [81]). By exploiting the symmetry inherent in the fracture tests, a quarter-model approach was employed, assuming linear-elastic material behavior (properties provided in Table 2). To address the high sensitivity of stress concentrations to mesh density, a refined mesh was implemented at the notch root, with the element size set to a fraction of the control volume radius. A preliminary mesh convergence analysis verified that stress evaluations achieve asymptotic stability within this refinement range (Figure 6). The FE models, shown in Figure 7, were constructed using element counts ranging from approximately 24,000 to 42,000 across the different notch radii.

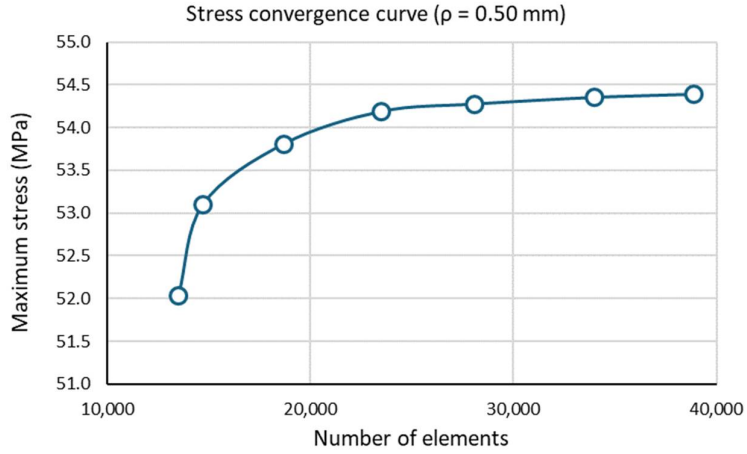

Figure 6. Stress convergence analysis for a representative notch radius (ρ = 0.50 mm).

The maximum principal stress at the notch root ($\sigma_{max\text{-}FE}$) was calculated for a reference external load of P_{FE} = 10 N. The corresponding critical load for each specimen was subsequently determined through linear proportionality, as defined by Equation (9). Although the stress field is highly sensitive to specimen geometry, particularly the notch radius, and acknowledging that actual dimensions may deviate from nominal values, a specific simulation was conducted for each specimen type to ensure analytical efficiency and accuracy.

$$P_{ASED} = P_{FE}\frac{\sigma_{max-ASED}}{\sigma_{max-FE}} \quad (9)$$

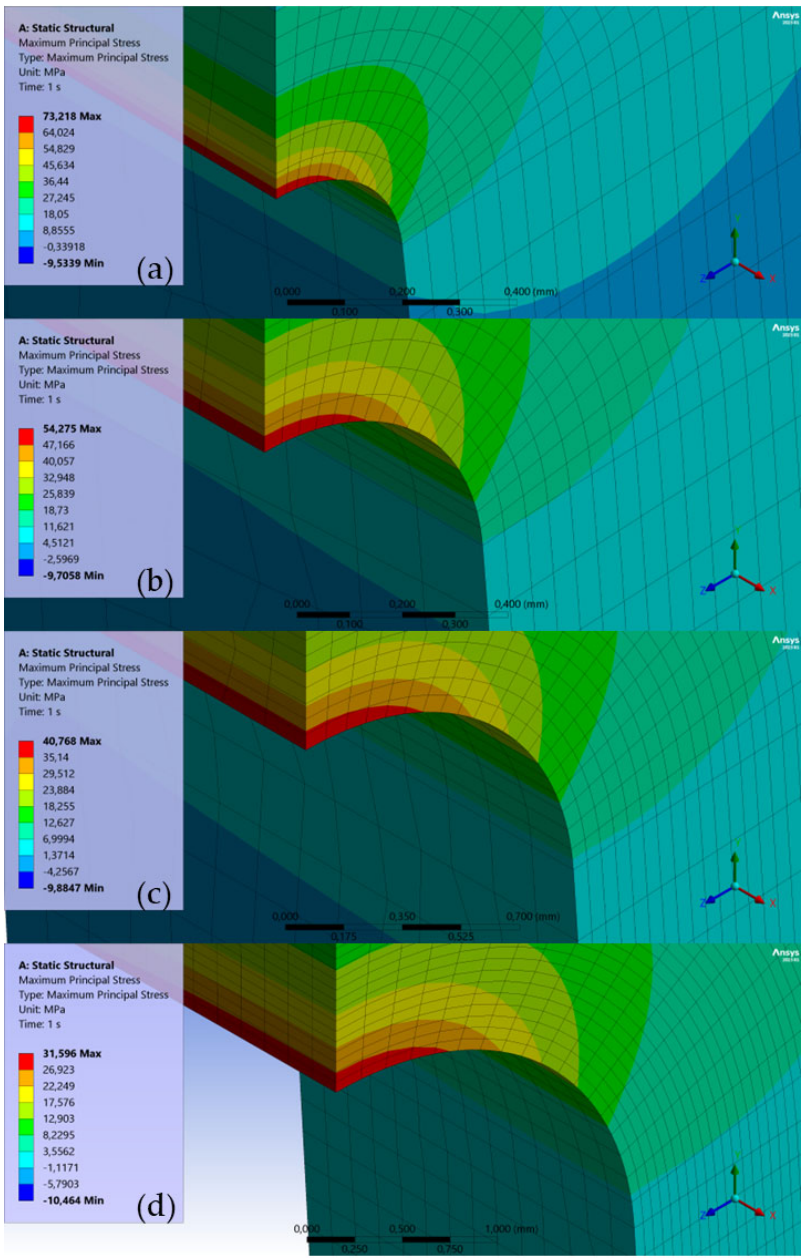

Figure 7. FE model for the investigated U-notched specimens: (**a**) ρ = 0.25 mm; (**b**) ρ = 0.50 mm; (**c**) ρ = 1.00 mm; and (**d**) ρ = 2.00 mm, subjected to a reference load P_{FE} = 10 N.

The experimental fracture loads, which correspond to the experimental maximum load (P_{max}), and the corresponding predictions derived from the ASED criterion (P_{ASED}) are presented in Appendix A (from Table A1 to Table A4). As illustrated in the Results and Discussion section, the standard ASED predictions (i.e., no calibration) are significant but consistently conservative. This arises because the materials under investigation exhibit significant non-linear tensile behavior, violating the linear-elastic assumption inherent to the standard ASED framework. To account for this, the criterion was calibrated by determining equivalent characteristic parameters, the critical strain energy density (W_C*) and the critical radius (R_C*) [55,60,65,68,70,82,83]. This calibration effectively models an "equivalent" linear-elastic material, enabling the application of the standard ASED formulation. The calibration process utilized the fracture loads obtained from conventional SENB specimens with varying U-notch radii. Specifically, fracture data from two distinct conditions, crack-like geometries and specimens with a 2.00 mm notch radius, were used to establish the

following relationships, based on the respective maximum stresses at the notch root (σ_{max1} and σ_{max2}):

$$F(2\alpha)H_1\left(2\alpha, \frac{R_C}{\rho}\right)\frac{{\sigma_{max1}}^2}{E} = W_C \quad (10)$$

$$F(2\alpha)H_2\left(2\alpha, \frac{R_C}{\rho}\right)\frac{{\sigma_{max2}}^2}{E} = W_C \quad (11)$$

The maximum stresses at their corresponding notch root, σ_{max1} and σ_{max2}, are obtained using the average fracture loads of each specimen configuration (defined by material, raster orientation, and notch radius). By providing various values of R_C in Equations (10) and (11), two distinct curves of W_C versus R_C were generated for the pure PEEK and fiber-reinforced composites. The intersection of these curves yields the unique calibrated material parameters, W_C* and R_C*, which implicitly account for the non-linear response of the materials.

Once the characteristic parameters are successfully calibrated, the fracture loads (P_{ASED}*) for arbitrary notch radii can be predicted straightforwardly. This is achieved by applying the standard linear-elastic ASED procedure using the calibrated parameters (W_C* and R_C*) rather than the values derived from the conventional non-calibrated procedure. Under this failure criterion, the critical maximum stress at the notch root ($\sigma_{max\text{-}ASED}$*) is determined by applying Equation (8). Finally, the predicted fracture load (P_{ASED}*) is obtained via linear proportionality, as defined by Equation (12):

$$P^*_{ASED} = P_{FE}\frac{\sigma^*_{max-ASED}}{\sigma_{max-FE}} \quad (12)$$

It is important to clarify the distinction between the numerical constitutive model and the failure evaluation framework: while the FE computations are performed within a linear-elastic framework, the calibration of the ASED parameters (W_C* and R_C*) permits applying this linear-elastic framework to materials that do not exhibit fully linear-elastic behavior.

3. Results and Discussion

3.1. Calibration of ASED Parameters and Analysis of Material Trends

Following the procedure described above, the initial critical strain energy density values (W_C) were calculated using the linear approximation of Equation (1), with Young's modulus (E) and ultimate tensile strength (σ_u) values obtained from Table 2. W_C results are presented in Table 4.

Applying the calibration procedure described previously, the intersection of the W_C versus R_C curves, derived from Equations (10) and (11), yields the unique calibrated material parameters W_C* and R_C*. As illustrated in Figure 8, these characteristic curves successfully capture the specific response of each material configuration, with the resulting calibrated values summarized in Table 4.

Regarding the crack-like baseline ($\rho = 0.00$ mm), these defects were introduced via a razor-blade sawing [72,73]. Due to inherent limitations of this technique, the actual notch-root radius of these razor-notched specimens exhibits a finite dimension of $\rho \approx 0.1$ mm, corresponding to the blade thickness. In this procedure, this razor-sharpened configuration was evaluated as a finite notch of $\rho = 0.10$ mm, using the corresponding $H(R_C/\rho)$ value in Equations (10) and (11). Because this radius is an order of magnitude smaller than the maximum evaluated notch radii (2.00 mm) and below the characteristic control volume scale (R_C*), minor deviations in the exact notch tip geometry have a negligible influence on the averaged strain energy within the control volume, thereby providing a consistent boundary condition for the calibration procedure.

Table 4. Summary of initial and calibrated critical strain energy density values (W_C and W_C*, respectively), alongside the calibrated critical radii (R_C*), for the investigated materials and raster orientations.

Material	RO	W_C (MPa)	W_C* (MPa)	R_C* (mm)
PEEK	0/90	0.671	2.153	0.44
	30/−60	0.797	4.586	0.22
	45/−45	0.682	4.679	0.18
PEEK-CF10	0/90	0.363	0.613	0.62
	30/−60	0.326	1.380	0.22
	45/−45	0.318	1.091	0.24
PEEK-CF20	0/90	0.402	1.770	0.18
	30/−60	0.149	2.144	0.16
	45/−45	0.359	2.802	0.14
PEEK-GF20	0/90	0.424	1.160	0.38
	30/−60	0.234	0.582	1.16
	45/−45	0.209	0.369	2.02

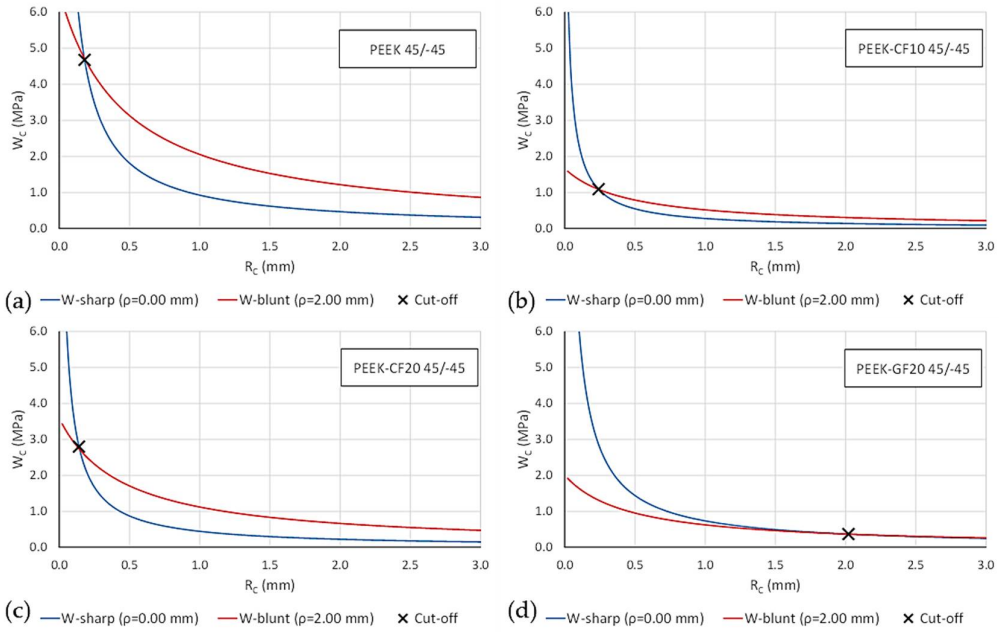

Figure 8. Calibration of the characteristic parameters W_C* and R_C* using SENB U-notched specimens: (**a**) PEEK 45/−45, (**b**) PEEK-CF10 45/−45, (**c**) PEEK-CF20 45/−45, and (**d**) PEEK-GF20 45/−45.

Figure 9 illustrates the calibrated ASED parameters across all evaluated materials and raster orientations. Neat PEEK exhibits the highest W_C* values, particularly at 30/−60 and 45/−45 raster orientations, reflecting superior energy absorption capacity compared to its fiber-reinforced alternatives. Increasing the carbon-fiber content from 10 wt.% to 20 wt.% increases W_C* and decreases R_C*, with PEEK-CF20 showing consistently the smallest control radii. The R_C* remain generally compact (≤0.6 mm) for most configurations, with the notable exception observed of PEEK-GF20, reaching 1.16 and 2.02 mm at 30/−60 and 45/−45, respectively. These contrasting trends indicate that the effect of raster orientation on the calibrated parameters depends on the reinforcement.

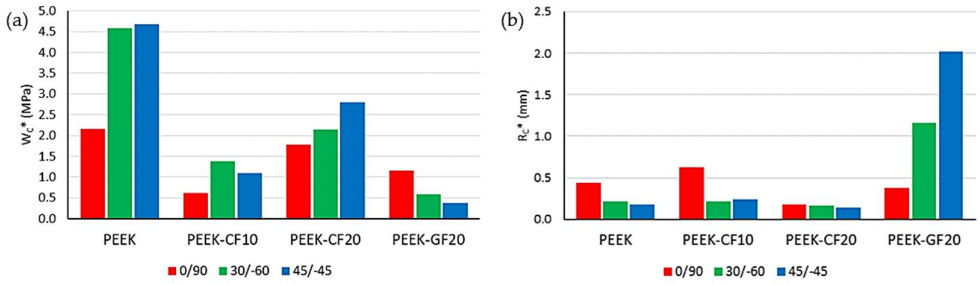

Figure 9. Calibrated parameters: (**a**) critical strain energy density (W_C^*) and (**b**) critical radius (R_C^*).

3.2. Fracture Load Predictions and Evaluation

A total of 240 FFF-printed SENB specimens were tested across all material configurations, with 48 specimens in the crack-like condition and 192 in notched configurations (0.25 mm, 0.50 mm, 1.00 mm, and 2.00 mm notch radii). From the notched tests, three results were discarded due to abnormally low fracture loads, most likely attributed to localized printing defects, resulting in a final validated dataset of 189 notched tests as detailed in Table 5. To evaluate the standard ASED criterion, predicted fracture loads (P_{ASED}) were compared against experimental values (P_{max}) (see Figures 10–13 and Tables A1–A4). The conventional approach significantly underestimates the fracture loads, yielding a mean P_{ASED}/P_{max} ratio of 0.677 for neat PEEK, 0.711 for PEEK-CF10, 0.665 for PEEK-CF20, and 0.760 for PEEK-GF20. This systematic underestimation confirms the conservatism of linear-elastic assumptions for these non-linear materials.

Table 5. Summary of statistical performance of the calibrated ASED criterion, comparing the overall dataset with the independent validation subset (ρ = 2.00 mm excluded, italicized rows).

Material	RO	N	Mean P_{ASED}^*/P_{max}	Std. Dev.	Max. P_{ASED}^*/P_{max}
PEEK	0/90	16	0.903	0.088	1.029
		12	*0.873*	*0.080*	*1.025*
	30/−60	16	0.858	0.106	1.122
		12	*0.813*	*0.066*	*0.926*
	45/−45	16	0.858	0.114	1.108
		12	*0.811*	*0.078*	*0.941*
PEEK-CF10	0/90	15	0.994	0.029	1.069
		11	*0.992*	*0.033*	*1.069*
	30/−60	16	0.892	0.094	1.107
		12	*0.857*	*0.071*	*0.985*
	45/−45	16	0.866	0.150	1.130
		12	*0.817*	*0.123*	*1.079*
PEEK-CF20	0/90	15	0.817	0.115	1.037
		12	*0.772*	*0.071*	*0.872*
	30/−60	16	0.926	0.240	1.498
		12	*0.884*	*0.212*	*1.234*
	45/−45	16	0.890	0.116	1.141
		12	*0.848*	*0.093*	*1.037*

Table 5. *Cont.*

Material	RO	N	Mean P_{ASED}^*/P_{max}	Std. Dev.	Max. P_{ASED}^*/P_{max}
PEEK-GF20	0/90	15	0.949	0.153	1.113
		11	*0.922*	*0.145*	*1.054*
	30/−60	16	1.008	0.048	1.090
		12	*1.010*	*0.054*	*1.090*
	45/−45	16	0.957	0.062	1.049
		12	*0.943*	*0.066*	*1.049*

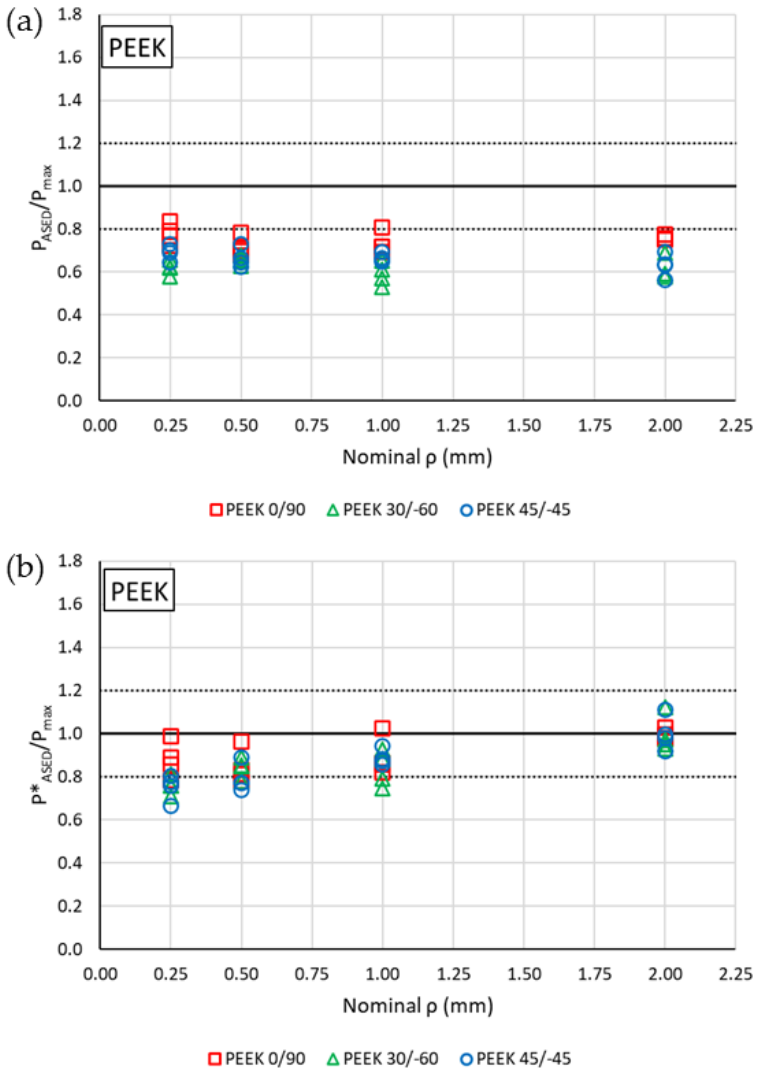

Figure 10. Comparison of experimental (P_{max}) and predicted fracture loads for neat PEEK specimens using: (**a**) the standard linear-elastic ASED criterion (P_{ASED}) and (**b**) the calibrated ASED criterion (P_{ASED}^*).

Calibration improves the predictive accuracy, shifting the results toward the experimental values while maintaining a conservative margin in most of the cases. The mean predicted-to-measured load ratio improves by 29% for PEEK and PEEK-CF10, 32% for PEEK-CF20, and 28% for PEEK-GF20, indicating a closer alignment of average predictions with experimental fracture loads. The increased dispersion in the prediction of PEEK-CF20 30/−60 raster orientation specimens, with some important overestimation results, is at-

tributed to higher variability in the experimental fracture data. As expected when applying the ASED criterion, the predictions are more reliable for raster orientations exhibiting brittle behavior, those closer to linear response, as confirmed by tensile results presented in Figure 3.

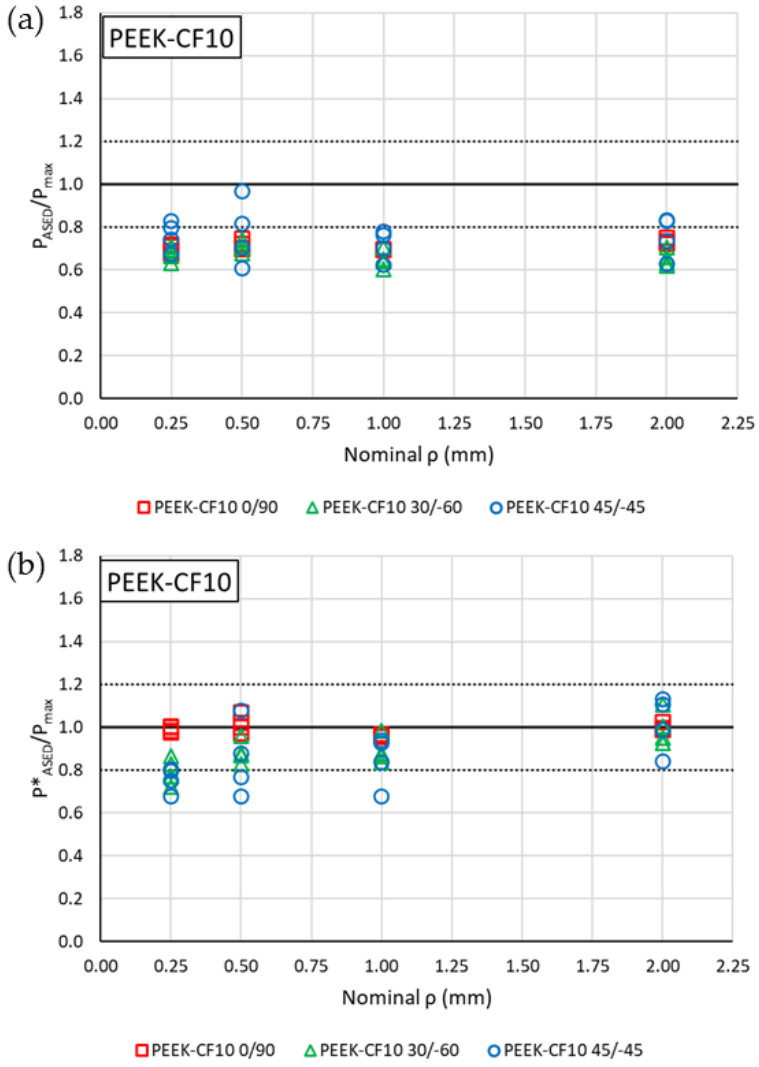

Figure 11. Comparison of experimental (P_{max}) and predicted fracture loads for PEEK-CF10 specimens using: (**a**) the standard linear-elastic ASED criterion (P_{ASED}) and (**b**) the calibrated ASED criterion (P_{ASED}*).

To rigorously quantify the performance of the calibrated ASED criterion, Table 5 details the statistical analysis for each material and raster orientation, explicitly distinguishing between the overall dataset and the independent validation subset (which excludes the 2.00 mm notch radius used for calibration). The approach successfully provides average predictions close to unity (ranging from 0.817 to 1.008 for all tests, and from 0.772 to 1.010 for the independent validation subset), across all configurations, demonstrating that it is capable of capturing the physics of the fracture process. This being said, and given the scatter observed in the experimental results (inherent to fracture processes), there are cases that exhibit non-conservative behavior (P_{ASED}*/P_{max} > 1). Specifically, non-conservative predictions occurred in 46 out of 189 valid tests (N) conducted on notched specimens across all evaluated configurations (25 out of 142 valid tests for the validation subset). These overestimations were predominantly concentrated under specific conditions: primarily at larger notch radii (1.00 mm and

2.00 mm), but without a particular influence of the raster orientation. Within the validation subset, the maximum overestimation observed reached a ratio of 1.234 for the PEEK-CF20 30/−60 configuration, whereas the absolute maximum overestimation across the entire dataset reached a ratio of 1.498 for the same material configuration. This diminished performance observed in this specific configuration is attributed to printing defects and suboptimal fabrication quality within those specific tensile specimens, rather than an inherent material limitation, as discussed in [73]. In any case, these type of results indicate, on the one hand, that the analysis correctly and safely predicts average fracture loads, but also that, in terms of design and assessment purposes, if conservative predictions are required for each individual case, additional safety factors would be required.

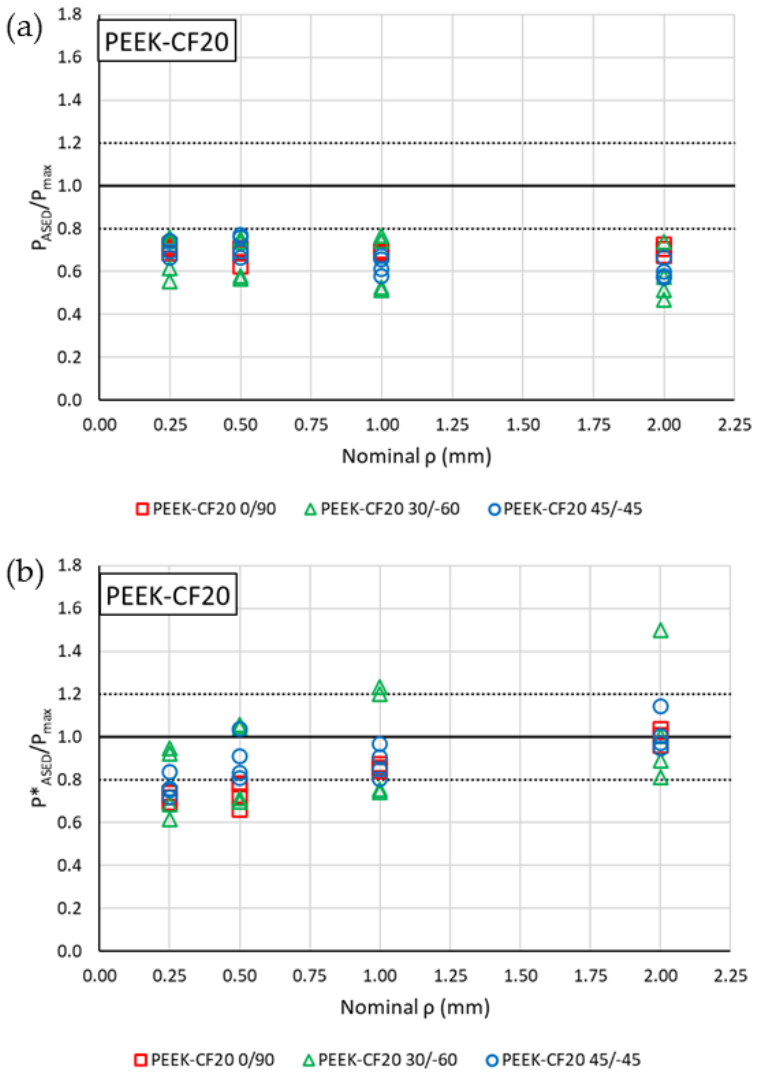

Figure 12. Comparison of experimental (P_{max}) and predicted fracture loads for PEEK-CF20 specimens using: (**a**) the standard linear-elastic ASED criterion (P_{ASED}) and (**b**) the calibrated ASED criterion (P_{ASED}*).

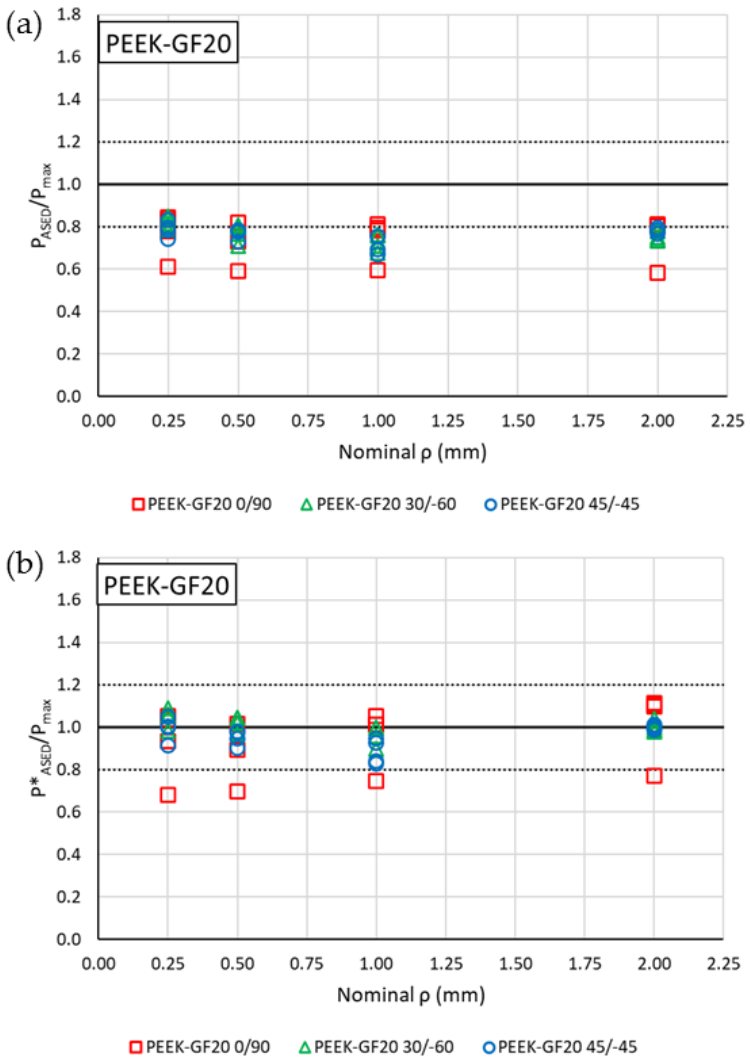

Figure 13. Comparison of experimental (P_{max}) and predicted fracture loads for PEEK-GF20 specimens using: (**a**) the standard linear-elastic ASED criterion (P_{ASED}) and (**b**) the calibrated ASED criterion (P_{ASED}*).

4. Conclusions

This study investigated the fracture behavior of neat PEEK and three fiber-reinforced composites (PEEK-CF10, PEEK-CF20, and PEEK-GF20) containing notches, focusing on the applicability of the calibrated ASED criterion in the presence of material non-linearity. Three raster orientations and five notch radii were investigated to assess the performance of the uncalibrated and calibrated formulations. It was demonstrated that the standard linear-elastic ASED approach significantly underestimates fracture loads for these materials, yielding mean P_{ASED}/P_{max} ratios from 0.665 to 0.760, respectively. These discrepancies were attributed to the pronounced non-linear tensile behavior observed across the tested raster orientations.

To mitigate these inaccuracies, an existing calibration procedure was applied and evaluated to determine equivalent characteristic parameters (critical strain energy density, W_C*, and critical radius, R_C*) using conventional 3D-printed SENB specimens. By incorporating these calibrated parameters, the ASED criterion was successfully extended to account for the non-linear response of the materials without requiring complex constitutive modeling. The results show that the proposed calibration leads to average P_{ASED}*/P_{max} ratios between 0.873 and 0.972 across the four evaluated materials, demonstrating the capacity of the approach to provide accurate predictions of fracture loads. Thus, the calibration procedure improved agreement with the experimental results while retaining linear-elastic finite ele-

ment analyses, without explicitly modeling non-linear constitutive behavior. The calibrated parameters depended on both material composition and raster orientation, supporting the use of material- and orientation-specific calibrations.

Overall, the results support extending the calibrated ASED criterion to the investigated high-performance, semi-crystalline FFF-printed PEEK and its fiber-reinforced composites, accounting for significant material non-linear behavior, providing a robust methodology across different fiber contents, notch geometries, and raster orientations. By utilizing the calibrated characteristic parameters (W_C* and R_C*), the proposed ASED calibration procedure effectively bridges the gap between linear-elastic theory and the observed non-linear behavior, supporting its use for fracture-load assessment within the investigated material, manufacturing, and loading conditions. Nonetheless, certain limitations should be emphasized: because the model assumes an idealized continuum, it cannot explicitly account for localized processing defects or isolated microstructural variations. Further work should quantify uncertainty in the calibrated parameters and assess their transferability to different geometries, thicknesses, and loading conditions before broader structural-design use is claimed. Additionally, the consideration of additional safety factors in the calibrated model should be analyzed when safe predictions are required in each individual fracture test, and not only in the average values.

Author Contributions: Conceptualization, S.A. and S.C.; methodology, S.A. and S.C.; validation, S.A. and S.C.; formal analysis, S.A. and S.C.; investigation, S.A. and S.C.; resources, S.C.; data curation, S.A.; writing—original draft preparation, S.A.; writing—review and editing, S.A. and S.C.; supervision, S.C.; funding acquisition, S.C. All authors have read and agreed to the published version of the manuscript.

Funding: This publication is part of the project "Comportamiento en fractura y efecto entalla en compuestos de matriz termoplástica obtenidos por fabricación aditiva, PID2021-122324NB-I00" funded by MCIN/AEI/10.13039/501100011033/FEDER "Una manera de hacer Europa".

Data Availability Statement: The original data presented in the study are openly available in [84–86].

Conflicts of Interest: The authors declare no conflicts of interest.

Abbreviations

The following abbreviations are used in this manuscript:

ABS	Acrylonitrile butadiene styrene
AM	Additive manufacturing
ASA	Acrylonitrile-styrene-acrylate
ASED	Average Strain Energy Density criterion
ASTM	American Society for Testing and Materials
FE	Finite element
FFF	Fused filament fabrication
MEX	Material extrusion
PEEK	Polyether-ether-ketone
PEEK-CF10	Carbon-fiber reinforced PEEK (10 wt.%)
PEEK-CF20	Carbon-fiber reinforced PEEK (20 wt.%)
PEEK-GF20	Glass-fiber reinforced PEEK (20 wt.%)
PLA	Polylactic acid
RO	Raster orientation
SENB	Single-edge-notched bending
TCD	Theory of Critical Distances

Appendix A

The appendix compiles the experimental fracture loads (P_{max}), the fracture load predictions obtained using the standard linear-elastic ASED criterion (P_{ASED}), and those obtained

using the calibrated ASED criterion (P_{ASED}*) for PEEK (Table A1) PEEK-CF10 (Table A2), PEEK-CF20 (Table A3), and PEEK-GF20 (Table A4).

Table A1. Experimental (P_{max}) and predicted (P_{ASED}) fracture loads for PEEK SENB specimens.

RO	Test nº	ρ (mm)	W (mm)	B (mm)	a_0 (mm)	P_{max} (N)	P_{ASED} (N)	P_{ASED}/P_{max}	P_{ASED}* (N)	P_{ASED}*/P_{max}
0/90	1	0.00	9.81	5.12	5.59	192.20	-	-	-	-
	2	0.00	9.79	4.96	5.20	199.86	-	-	-	-
	3	0.00	9.74	4.99	5.51	240.74	-	-	-	-
	4	0.00	9.76	4.95	5.60	174.29	-	-	-	-
	1	0.25	9.79	4.71	4.95	246.31	178.01	0.723	192.81	0.783
	2	0.25	9.78	4.91	4.89	216.34	171.29	0.792	192.81	0.891
	3	0.25	9.71	5.13	4.85	195.40	163.30	0.836	192.81	0.987
	4	0.25	9.77	4.86	4.99	224.83	172.50	0.767	192.81	0.858
	1	0.50	9.74	5.09	4.60	201.55	158.02	0.784	194.16	0.963
	2	0.50	9.77	4.96	4.51	239.14	166.74	0.697	194.16	0.812
	3	0.50	9.76	4.89	4.56	249.70	169.54	0.679	194.16	0.778
	4	0.50	9.82	4.86	4.57	232.78	164.86	0.708	194.16	0.834
	1	1.00	9.76	4.86	4.80	244.41	169.65	0.694	200.67	0.821
	2	1.00	9.76	5.02	4.80	234.30	168.10	0.717	200.67	0.856
	3	1.00	9.78	5.21	4.84	231.90	166.92	0.720	200.67	0.865
	4	1.00	9.73	5.12	4.67	195.75	157.97	0.807	200.67	1.025
	1	2.00	9.78	4.99	4.80	217.16	163.49	0.753	212.00	0.976
	2	2.00	9.77	4.89	4.75	216.77	162.98	0.752	212.00	0.978
	3	2.00	9.78	5.14	4.57	205.96	156.10	0.758	212.00	1.029
	4	2.00	9.83	4.93	4.87	212.60	164.57	0.774	212.00	0.997
30/−60	1	0.00	9.77	5.12	5.34	188.49	-	-	-	-
	2	0.00	9.78	5.06	4.53	298.07	-	-	-	-
	3	0.00	9.81	5.06	6.35	134.88	-	-	-	-
	4	0.00	9.87	5.04	6.33	138.79	-	-	-	-
	1	0.25	9.80	5.00	4.47	263.57	152.04	0.577	187.18	0.710
	2	0.25	9.75	5.16	4.69	230.66	151.86	0.658	187.18	0.811
	3	0.25	9.79	5.12	4.72	246.24	152.86	0.621	187.18	0.760
	4	0.25	9.77	4.92	4.52	247.34	154.26	0.624	187.18	0.757
	1	0.50	9.77	4.95	4.69	231.49	151.74	0.655	196.03	0.847
	2	0.50	9.78	4.96	4.74	250.94	157.82	0.629	196.03	0.781
	3	0.50	9.75	5.10	4.71	220.33	148.82	0.675	196.03	0.890
	4	0.50	9.77	4.95	4.93	230.25	149.90	0.651	196.03	0.851
	1	1.00	9.77	5.07	4.73	242.32	148.59	0.613	213.68	0.882
	2	1.00	9.76	5.01	4.81	269.90	154.05	0.571	213.68	0.792
	3	1.00	9.78	4.98	4.62	286.73	151.88	0.530	213.68	0.745
	4	1.00	9.74	5.18	4.84	230.74	150.98	0.654	213.68	0.926
	1	2.00	9.77	4.95	4.78	257.16	148.91	0.579	239.44	0.931
	2	2.00	9.77	5.18	4.94	213.46	147.39	0.690	239.44	1.122
	3	2.00	9.79	5.12	5.00	252.29	149.12	0.591	239.44	0.949
	4	2.00	9.77	4.98	4.77	246.27	145.50	0.591	239.44	0.972
45/−45	1	0.00	9.79	4.88	4.62	297.34	-	-	-	-
	2	0.00	9.79	5.19	5.06	241.49	-	-	-	-
	3	0.00	9.83	5.04	6.97	77.77	-	-	-	-
	4	0.00	9.96	5.26	7.42	119.98	-	-	-	-
	1	0.25	9.75	5.18	5.05	227.82	166.57	0.731	183.55	0.806
	2	0.25	9.78	4.98	4.80	275.59	177.51	0.644	183.55	0.666
	3	0.25	9.76	4.98	4.51	237.07	166.38	0.702	183.55	0.774
	4	0.25	9.78	4.95	4.62	241.93	166.77	0.689	183.55	0.759
	1	0.50	9.85	4.86	4.76	252.99	163.19	0.645	194.97	0.771
	2	0.50	9.79	4.85	4.68	252.30	167.20	0.663	194.97	0.773
	3	0.50	9.82	5.11	4.79	263.86	164.83	0.625	194.97	0.739
	4	0.50	9.82	5.17	4.68	218.91	160.01	0.731	194.97	0.891
	1	1.00	9.79	4.81	4.89	247.01	160.90	0.651	216.18	0.875
	2	1.00	9.77	5.15	4.92	229.79	159.62	0.695	216.18	0.941
	3	1.00	9.75	4.93	4.88	251.98	163.88	0.650	216.18	0.858
	4	1.00	9.79	5.04	5.06	245.75	162.85	0.663	216.18	0.880
	1	2.00	9.78	5.01	4.78	247.32	156.43	0.632	246.21	0.996
	2	2.00	9.72	5.02	3.98	267.64	150.37	0.562	246.21	0.920
	3	2.00	9.76	5.21	4.81	222.13	154.14	0.694	246.21	1.108
	4	2.00	9.78	4.82	5.13	251.19	159.74	0.636	246.21	0.980

Table A2. Experimental (P_{max}) and predicted (P_{ASED}) fracture loads for PEEK-CF10 SENB specimens.

RO	Test nº	ρ (mm)	W (mm)	B (mm)	a_0 (mm)	P_{max} (N)	P_{ASED} (N)	P_{ASED}/P_{max}	P_{ASED}* (N)	P_{ASED}*/P_{max}
0/90	1	0.00	9.78	5.14	4.81	119.08	-	-	-	-
	2	0.00	9.81	5.03	4.71	180.37	-	-	-	-
	3	0.00	9.77	5.03	4.99	167.73	-	-	-	-
	4	0.00	9.78	4.94	4.69	181.11	-	-	-	-
	1	0.25	9.80	5.94	4.81	157.19	105.91	0.674	153.37	0.976
	2	0.25	9.82	5.02	4.52	152.65	108.52	0.711	153.37	1.005
	3	0.25	9.75	5.16	5.07	153.51	110.05	0.717	153.37	0.999
	4	0.25	9.77	4.98	4.60	155.80	107.52	0.690	153.37	0.984
	1	0.50	9.81	5.10	4.88	142.54	106.26	0.745	152.32	1.069
	2	0.50	9.80	5.12	4.71	149.15	107.51	0.721	152.32	1.021
	3	0.50	9.80	5.01	4.72	152.18	105.99	0.696	152.32	1.001
	4	0.50	9.83	4.96	4.98	156.54	110.05	0.703	152.32	0.973
	1	1.00	9.75	5.09	4.61	160.47	111.40	0.694	154.11	0.960
	2	1.00	9.74	4.97	4.68	-	-	-	-	-
	3	1.00	9.80	4.99	4.95	159.67	111.08	0.696	154.11	0.965
	4	1.00	9.72	4.93	4.75	161.35	111.62	0.692	154.11	0.955
	1	2.00	9.70	5.06	4.91	158.96	115.79	0.728	158.36	0.996
	2	2.00	9.84	5.02	4.95	160.23	115.89	0.723	158.36	0.988
	3	2.00	9.75	4.96	4.87	160.24	117.40	0.733	158.36	0.988
	4	2.00	9.68	5.10	4.86	154.42	115.66	0.749	158.36	1.026
30/−60	1	0.00	9.89	4.91	6.05	123.38	-	-	-	-
	2	0.00	9.81	4.93	5.31	154.78	-	-	-	-
	3	0.00	9.83	4.95	4.88	197.20	-	-	-	-
	4	0.00	9.82	5.21	6.61	75.64	-	-	-	-
	1	0.25	9.80	4.93	4.36	163.65	113.69	0.695	135.66	0.829
	2	0.25	9.79	5.21	4.77	157.10	111.30	0.708	135.66	0.864
	3	0.25	9.85	4.96	4.69	188.14	118.81	0.631	135.66	0.721
	4	0.25	9.84	4.97	4.74	175.71	116.96	0.666	135.66	0.772
	1	0.50	9.78	5.07	4.65	148.20	109.73	0.740	142.08	0.959
	2	0.50	9.80	4.97	4.88	162.02	115.00	0.710	142.08	0.877
	3	0.50	9.79	4.94	4.79	171.54	115.84	0.675	142.08	0.828
	4	0.50	9.80	4.91	4.87	163.63	115.35	0.705	142.08	0.868
	1	1.00	9.76	4.93	4.68	176.27	114.48	0.649	154.88	0.879
	2	1.00	9.78	5.16	4.89	157.23	110.71	0.704	154.88	0.985
	3	1.00	9.80	4.83	4.72	179.29	115.04	0.642	154.88	0.864
	4	1.00	9.74	4.91	4.33	185.49	111.67	0.602	154.88	0.835
	1	2.00	9.79	4.92	4.77	187.11	116.07	0.620	173.54	0.927
	2	2.00	9.82	4.91	4.82	182.88	115.27	0.630	173.54	0.949
	3	2.00	9.80	5.15	4.79	156.79	110.80	0.707	173.54	1.107
	4	2.00	9.80	4.92	4.81	172.77	113.84	0.659	173.54	1.004
45/−45	1	0.00	9.76	4.25	5.99	97.96	-	-	-	-
	2	0.00	9.86	5.47	5.28	138.18	-	-	-	-
	3	0.00	9.74	4.36	5.73	112.85	-	-	-	-
	4	0.00	9.78	4.29	5.75	110.04	-	-	-	-
	1	0.25	9.81	4.26	4.87	150.14	111.63	0.744	112.49	0.749
	2	0.25	9.68	5.39	4.69	166.42	111.87	0.672	112.49	0.676
	3	0.25	9.77	3.93	4.77	141.75	112.62	0.794	112.49	0.794
	4	0.25	9.79	3.86	5.30	139.85	115.70	0.827	112.49	0.804
	1	0.50	9.78	4.35	4.61	108.57	104.78	0.965	117.13	1.079
	2	0.50	9.76	3.98	4.69	133.63	109.12	0.817	117.13	0.877
	3	0.50	9.73	4.26	4.49	152.96	107.81	0.705	117.13	0.766
	4	0.50	9.75	5.26	4.39	173.29	105.37	0.608	117.13	0.676
	1	1.00	9.79	4.28	4.94	187.51	117.11	0.625	126.76	0.676
	2	1.00	9.70	3.94	4.50	151.20	105.82	0.700	126.76	0.838
	3	1.00	9.72	4.01	4.32	135.24	103.25	0.763	126.76	0.937
	4	1.00	9.79	3.89	4.76	136.64	106.71	0.781	126.76	0.928
	1	2.00	9.71	4.33	4.67	142.88	104.95	0.735	141.01	0.987
	2	2.00	9.79	3.88	4.94	127.71	106.47	0.834	141.01	1.104
	3	2.00	9.83	5.33	4.97	168.07	105.23	0.626	141.01	0.839
	4	2.00	9.71	3.91	4.70	124.79	103.32	0.828	141.01	1.130

Table A3. Experimental (P_{max}) and predicted (P_{ASED}) fracture loads for PEEK-CF20 SENB specimens.

RO	Test nº	ρ (mm)	W (mm)	B (mm)	a_0 (mm)	P_{max} (N)	P_{ASED} (N)	P_{ASED}/P_{max}	P_{ASED}* (N)	P_{ASED}*/P_{max}
0/90	1	0.00	9.92	4.86	6.87	85.10	-	-	-	-
	2	0.00	9.94	5.16	5.52	220.36	-	-	-	-
	3	0.00	9.90	4.92	4.68	324.01	-	-	-	-
	4	0.00	9.85	4.91	6.38	140.05	-	-	-	-
	1	0.25	9.84	4.94	4.89	267.83	188.90	0.705	191.75	0.716
	2	0.25	9.92	4.97	5.18	259.86	189.09	0.728	191.75	0.738
	3	0.25	9.88	5.03	4.90	276.57	189.19	0.684	191.75	0.693
	4	0.25	9.88	5.02	4.80	259.83	185.82	0.715	191.75	0.738
	1	0.50	9.92	4.87	4.92	307.83	191.42	0.622	203.69	0.662
	2	0.50	9.79	4.93	4.75	259.42	182.93	0.705	203.69	0.785
	3	0.50	9.78	4.92	4.82	260.92	185.67	0.712	203.69	0.781
	4	0.50	9.94	4.95	5.35	281.57	193.38	0.687	203.69	0.723
	1	1.00	9.89	5.04	4.80	258.90	180.49	0.697	225.85	0.872
	2	1.00	9.88	4.99	4.77	264.76	181.51	0.686	225.85	0.853
	3	1.00	9.96	5.18	4.96	263.93	183.45	0.695	225.85	0.856
	4	1.00	9.93	4.97	5.04	268.14	184.44	0.688	225.85	0.842
	1	2.00	9.88	4.94	5.02	255.19	180.33	0.707	257.22	1.008
	2	2.00	9.81	5.05	4.90	248.00	180.36	0.727	257.22	1.037
	3	2.00	9.86	5.09	4.82	-	-	-	-	-
	4	2.00	9.93	4.97	4.82	268.76	181.32	0.675	257.22	0.957
30/−60	1	0.00	9.75	5.10	4.89	-	-	-	-	-
	2	0.00	9.74	5.02	5.39	130.24	-	-	-	-
	3	0.00	9.76	5.07	5.35	141.11	-	-	-	-
	4	0.00	9.84	4.94	6.09	-	-	-	-	-
	1	0.25	9.88	5.13	4.94	221.22	122.78	0.555	136.30	0.616
	2	0.25	9.83	5.00	4.66	143.86	109.00	0.758	136.30	0.947
	3	0.25	9.77	5.12	4.61	199.29	122.78	0.616	136.30	0.684
	4	0.25	9.70	4.95	4.62	147.64	109.87	0.744	136.30	0.923
	1	0.50	9.79	4.98	4.86	138.37	104.31	0.754	146.07	1.056
	2	0.50	9.84	5.10	5.06	209.55	118.43	0.565	146.07	0.697
	3	0.50	9.87	5.07	4.85	204.91	118.43	0.578	146.07	0.713
	4	0.50	9.77	4.94	4.61	139.89	103.12	0.737	146.07	1.044
	1	1.00	9.80	5.16	4.89	216.61	113.92	0.526	163.60	0.755
	2	1.00	9.77	5.08	4.56	220.64	113.28	0.513	163.60	0.741
	3	1.00	9.77	4.95	4.81	132.62	101.70	0.767	163.60	1.234
	4	1.00	9.76	4.90	4.85	136.45	101.12	0.741	163.60	1.199
	1	2.00	9.75	5.09	4.72	187.47	107.43	0.573	188.04	1.003
	2	2.00	9.75	5.04	4.87	210.97	108.23	0.513	188.04	0.891
	3	2.00	9.81	5.18	4.98	231.45	108.23	0.468	188.04	0.812
	4	2.00	9.70	4.95	4.85	125.52	92.88	0.740	188.04	1.498
45/−45	1	0.00	9.87	4.96	6.47	155.68	-	-	-	-
	2	0.00	9.93	5.00	4.35	294.59	-	-	-	-
	3	0.00	9.94	4.90	5.44	205.58	-	-	-	-
	4	0.00	10.05	5.03	6.01	116.70	-	-	-	-
	1	0.25	9.85	4.95	5.47	257.67	191.43	0.743	195.89	0.760
	2	0.25	9.83	5.13	4.61	272.32	180.59	0.663	195.89	0.719
	3	0.25	9.94	4.95	4.87	260.34	180.55	0.694	195.89	0.752
	4	0.25	9.92	4.93	4.88	233.73	173.83	0.744	195.89	0.838
	1	0.50	9.87	5.00	4.21	204.58	157.80	0.771	212.14	1.037
	2	0.50	9.86	5.05	5.20	233.06	176.85	0.759	212.14	0.910
	3	0.50	9.88	4.96	4.81	254.83	176.99	0.695	212.14	0.832
	4	0.50	9.85	4.98	4.75	263.14	175.24	0.666	212.14	0.806
	1	1.00	9.86	5.02	4.79	283.63	173.20	0.611	240.33	0.847
	2	1.00	9.92	5.05	4.82	299.76	173.83	0.580	240.33	0.802
	3	1.00	9.82	5.02	4.73	248.85	167.60	0.673	240.33	0.966
	4	1.00	9.97	4.98	4.87	264.80	173.42	0.655	240.33	0.908
	1	2.00	9.95	4.98	4.95	295.00	168.92	0.573	279.00	0.946
	2	2.00	10.01	5.06	4.98	277.51	165.77	0.597	279.00	1.005
	3	2.00	9.92	4.97	4.82	286.87	166.10	0.579	279.00	0.973
	4	2.00	9.84	5.02	4.74	244.53	163.00	0.667	279.00	1.141

Table A4. Experimental (P_{max}) and predicted (P_{ASED}) fracture loads for PEEK-GF20 SENB specimens.

RO	Test nº	ρ (mm)	W (mm)	B (mm)	a_0 (mm)	P_{max} (N)	P_{ASED} (N)	P_{ASED}/P_{max}	P_{ASED}* (N)	P_{ASED}*/P_{max}
0/90	1	0.00	9.85	4.91	4.28	236.71	-	-	-	-
	2	0.00	10.03	5.07	5.25	213.20	-	-	-	-
	3	0.00	10.08	4.79	4.79	156.06	-	-	-	-
	4	0.00	9.89	4.98	6.70	95.77	-	-	-	-
	1	0.25	9.86	5.01	4.68	159.84	134.85	0.844	168.50	1.054
	2	0.25	9.90	5.00	4.95	180.18	140.34	0.779	168.50	0.935
	3	0.25	9.97	5.26	5.14	246.92	151.41	0.613	168.50	0.682
	4	0.25	9.86	4.94	4.75	162.37	135.13	0.832	168.50	1.038
	1	0.50	9.91	4.92	4.90	-	-	-	-	-
	2	0.50	9.88	4.98	5.16	168.07	137.69	0.819	170.87	1.017
	3	0.50	9.99	5.22	4.89	244.91	144.62	0.591	170.87	0.698
	4	0.50	9.86	4.84	4.68	190.82	139.49	0.731	170.87	0.895
	1	1.00	9.92	4.99	5.07	176.62	138.37	0.783	178.42	1.010
	2	1.00	9.92	5.00	5.04	169.52	137.94	0.814	178.42	1.053
	3	1.00	10.01	5.30	4.69	238.52	141.56	0.594	178.42	0.748
	4	1.00	9.87	4.87	5.08	176.34	140.17	0.795	178.42	1.012
	1	2.00	9.93	5.08	4.95	172.27	138.88	0.806	190.85	1.108
	2	2.00	10.06	5.10	4.73	247.57	144.61	0.584	190.85	0.771
	3	2.00	9.83	4.89	4.91	173.76	139.62	0.804	190.85	1.098
	4	2.00	9.94	4.83	4.93	171.43	139.50	0.814	190.85	1.113
30/−60	1	0.00	9.92	5.03	6.25	132.80	-	-	-	-
	2	0.00	9.97	5.00	5.13	180.87	-	-	-	-
	3	0.00	9.88	5.01	4.95	189.41	-	-	-	-
	4	0.00	9.88	5.13	4.21	222.41	-	-	-	-
	1	0.25	9.84	5.10	4.80	159.80	130.27	0.815	169.65	1.062
	2	0.25	9.88	4.96	5.00	172.45	135.53	0.786	169.65	0.984
	3	0.25	9.84	4.95	5.23	160.90	136.63	0.849	169.65	1.054
	4	0.25	9.89	5.06	4.76	155.59	130.97	0.842	169.65	1.090
	1	0.50	9.90	4.97	4.72	158.59	126.30	0.796	165.57	1.044
	2	0.50	9.83	5.18	3.96	170.13	120.58	0.709	165.57	0.973
	3	0.50	9.86	5.03	4.51	162.59	124.65	0.767	165.57	1.018
	4	0.50	9.88	5.09	4.82	158.46	127.83	0.807	165.57	1.045
	1	1.00	9.86	5.11	4.63	181.49	122.85	0.677	162.67	0.896
	2	1.00	9.85	4.89	4.83	163.67	124.06	0.758	162.67	0.994
	3	1.00	9.85	4.95	4.91	162.79	124.42	0.764	162.67	0.999
	4	1.00	9.85	4.95	4.54	169.93	120.77	0.711	162.67	0.957
	1	2.00	9.87	4.97	4.96	162.45	119.21	0.734	160.12	0.986
	2	2.00	9.91	5.03	4.97	153.97	120.07	0.780	160.12	1.040
	3	2.00	9.86	4.94	4.86	159.90	119.85	0.750	160.12	1.001
	4	2.00	9.84	5.14	5.16	163.67	121.07	0.740	160.12	0.978
45/−45	1	0.00	9.70	4.96	5.27	149.56	-	-	-	-
	2	0.00	9.87	5.29	4.78	206.52	-	-	-	-
	3	0.00	9.85	5.02	5.38	152.82	-	-	-	-
	4	0.00	9.87	4.94	5.44	176.05	-	-	-	-
	1	0.25	9.84	5.29	4.68	174.26	129.08	0.741	159.22	0.914
	2	0.25	9.83	5.01	4.68	158.64	125.90	0.794	159.22	1.004
	3	0.25	9.84	4.93	4.75	159.23	124.70	0.783	159.22	1.000
	4	0.25	9.82	4.99	4.79	151.78	126.61	0.834	159.22	1.049
	1	0.50	9.83	5.02	4.47	171.06	125.23	0.732	153.95	0.900
	2	0.50	9.77	5.35	4.68	157.19	123.02	0.783	153.95	0.979
	3	0.50	9.82	4.99	4.71	162.28	125.67	0.774	153.95	0.949
	4	0.50	9.84	5.06	4.56	157.70	123.20	0.781	153.95	0.976
	1	1.00	9.86	4.98	4.75	157.08	118.46	0.754	148.74	0.947
	2	1.00	9.83	4.86	4.84	160.32	121.09	0.755	148.74	0.928
	3	1.00	9.86	5.00	4.65	179.89	124.60	0.693	148.74	0.827
	4	1.00	9.84	5.27	4.61	177.13	118.18	0.667	148.74	0.840
	1	2.00	9.79	4.92	4.90	140.57	111.56	0.794	142.40	1.013
	2	2.00	9.82	5.19	4.83	143.94	110.12	0.765	142.40	0.989
	3	2.00	9.86	4.97	4.95	141.70	110.86	0.782	142.40	1.005
	4	2.00	9.82	4.93	4.80	143.21	111.92	0.781	142.40	0.994

References

1. Guo, N.; Leu, M.C. Additive Manufacturing: Technology, Applications and Research Needs. *Front. Mech. Eng.* **2013**, *8*, 215–243. [CrossRef]
2. Mwema, F.M.; Akinlabi, E.T. Basics of Fused Deposition Modelling (FDM). In *Fused Deposition Modeling: Strategies for Quality Enhancement*; Springer: Berlin/Heidelberg, Germany, 2020; pp. 1–15. [CrossRef]
3. Wickramasinghe, S.; Do, T.; Tran, P. FDM-Based 3D Printing of Polymer and Associated Composite: A Review on Mechanical Properties, Defects and Treatments. *Polymers* **2020**, *12*, 1529. [CrossRef]
4. Wang, P.; Zou, B.; Xiao, H.; Ding, S.; Huang, C. Effects of Printing Parameters of Fused Deposition Modeling on Mechanical Properties, Surface Quality, and Microstructure of PEEK. *J. Mater. Process. Technol.* **2019**, *271*, 62–74. [CrossRef]
5. Rinaldi, M.; Cecchini, F.; Pigliaru, L.; Ghidini, T.; Lumaca, F.; Nanni, F. Additive Manufacturing of Polyether Ether Ketone (PEEK) for Space Applications: A Nanosat Polymeric Structure. *Polymers* **2020**, *13*, 11. [CrossRef]
6. Naganaboyina, H.P.S.; Nagaraju, P.; Sonaye, S.Y.; Bokam, V.K.; Sikder, P. In-House Processing of Carbon Fiber-Reinforced Polyetheretherketone (CFR-PEEK) 3D Printable Filaments and Fused Filament Fabrication-3D Printing of CFR-PEEK Parts. *Int. J. Adv. Manuf. Technol.* **2023**, *128*, 5011–5024. [CrossRef]
7. Wu, Y.; Cao, Y.; Wu, Y.; Li, D. Neutron Shielding Performance of 3D-Printed Boron Carbide PEEK Composites. *Materials* **2020**, *13*, 2314. [CrossRef]
8. Dallal, S.; Eslami, B.; Tiari, S. Recent Advances in PEEK for Biomedical Applications: A Comprehensive Review of Material Properties, Processing, and Additive Manufacturing. *Polymers* **2025**, *17*, 1968. [CrossRef]
9. Zhao, F.; Li, D.; Jin, Z. Preliminary Investigation of Poly-Ether-Ether-Ketone Based on Fused Deposition Modeling for Medical Applications. *Materials* **2018**, *11*, 288. [CrossRef]
10. Rendas, P.; Figueiredo, L.; Machado, C.; Mourão, A.; Vidal, C.; Soares, B. Mechanical Performance and Bioactivation of 3D-Printed PEEK for High-Performance Implant Manufacture: A Review. *Prog. Biomater.* **2023**, *12*, 89–111. [CrossRef]
11. Ning, F.; Cong, W.; Qiu, J.; Wei, J.; Wang, S. Additive Manufacturing of Carbon Fiber Reinforced Thermoplastic Composites Using Fused Deposition Modeling. *Compos. Part B Eng.* **2015**, *80*, 369–378. [CrossRef]
12. Gonçalves, J.; Lima, P.; Krause, B.; Pötschke, P.; Lafont, U.; Gomes, J.R.; Abreu, C.S.; Paiva, M.C.; Covas, J.A. Electrically Conductive Polyetheretherketone Nanocomposite Filaments: From Production to Fused Deposition Modeling. *Polymers* **2018**, *10*, 925. [CrossRef]
13. Abu Bakar, M.S.; Cheng, M.H.W.; Tang, S.M.; Yu, S.C.; Liao, K.; Tan, C.T.; Khor, K.A.; Cheang, P. Tensile Properties, Tension–Tension Fatigue and Biological Response of Polyetheretherketone–Hydroxyapatite Composites for Load-Bearing Orthopedic Implants. *Biomaterials* **2003**, *24*, 2245–2250. [CrossRef]
14. Manzoor, F.; Golbang, A.; Jindal, S.; Dixon, D.; McIlhagger, A.; Harkin-Jones, E.; Crawford, D.; Mancuso, E. 3D Printed PEEK/HA Composites for Bone Tissue Engineering Applications: Effect of Material Formulation on Mechanical Performance and Bioactive Potential. *J. Mech. Behav. Biomed. Mater.* **2021**, *121*, 104601. [CrossRef]
15. Oladapo, B.I.; Zahedi, S.A. Improving Bioactivity and Strength of PEEK Composite Polymer for Bone Application. *Mater. Chem. Phys.* **2021**, *266*, 124485. [CrossRef]
16. El Magri, A.; Vanaei, S.; Vaudreuil, S. An Overview on the Influence of Process Parameters through the Characteristic of 3D-Printed PEEK and PEI Parts. *High. Perform. Polym.* **2021**, *33*, 862–880. [CrossRef]
17. Pulipaka, A.; Gide, K.M.; Beheshti, A.; Bagheri, Z.S. Effect of 3D Printing Process Parameters on Surface and Mechanical Properties of FFF-Printed PEEK. *J. Manuf. Process* **2023**, *85*, 368–386. [CrossRef]
18. Gupta, V.; Kulkarni, D.M.; Thiruselvam, I.; Chaudhari, V.V.; Pawar, R.; Suraj, S. Applications of 3D-Printed Polyether Ether Ketone and Its Composites. In *PEEK Blends and Composites*; Elsevier: Amsterdam, The Netherlands, 2026; pp. 397–418. [CrossRef]
19. Han, X.; Yang, D.; Yang, C.; Spintzyk, S.; Scheideler, L.; Li, P.; Li, D.; Geis-Gerstorfer, J.; Rupp, F. Carbon Fiber Reinforced PEEK Composites Based on 3D-Printing Technology for Orthopedic and Dental Applications. *J. Clin. Med.* **2019**, *8*, 240. [CrossRef]
20. Wang, P.; Zou, B.; Ding, S.; Huang, C.; Shi, Z.; Ma, Y.; Yao, P. Preparation of Short CF/GF Reinforced PEEK Composite Filaments and Their Comprehensive Properties Evaluation for FDM-3D Printing. *Compos. Part B Eng.* **2020**, *198*, 108175. [CrossRef]
21. Wang, P.; Zou, B.; Ding, S.; Li, L.; Huang, C. Effects of FDM-3D Printing Parameters on Mechanical Properties and Microstructure of CF/PEEK and GF/PEEK. *Chin. J. Aeronaut.* **2021**, *34*, 236–246. [CrossRef]
22. Yap, T.; Heathman, N.; Phillips, T.; Beaman, J.; Tehrani, M. Additive Manufacturing of Polyaryletherketone (PAEK) Polymers and Their Composites. *Compos. Part B Eng.* **2023**, *266*, 111019. [CrossRef]
23. Hu, Z.; He, J.; Chen, W.; Liu, W.; Ding, J.; He, C.; Wang, S.; Ning, F.; Li, X. High-Performance Carbon Fiber Reinforced Polyether-Ether-Ketone Composite Pellets 3D-Printed via Screw-Extrusion Additive Manufacturing. *Compos. Sci. Technol.* **2024**, *246*, 110362. [CrossRef]
24. Wei, S.; Deng, Y.; Liu, X.; Xu, A.; Wang, L.; Luo, Z.; Zheng, Y.; Deng, F.; Tang, Z.; Wei, J. Effect of Surface Roughness on Osteogenesis in Vitro and Osseointegration in Vivo of Carbon Fiber-Reinforced Polyetheretherketone-Nanohydroxyapatite Composite. *Int. J. Nanomed.* **2015**, *10*, 1425–1447. [CrossRef]

25. Jiang, N.; Tan, P.; He, M.; Zhang, J.; Sun, D.; Zhu, S. Graphene Reinforced Polyether Ether Ketone Nanocomposites for Bone Repair Applications. *Polym. Test.* **2021**, *100*, 107276. [CrossRef]
26. Wu, W.; Geng, P.; Li, G.; Zhao, D.; Zhang, H.; Zhao, J. Influence of Layer Thickness and Raster Angle on the Mechanical Properties of 3D-Printed PEEK and a Comparative Mechanical Study between PEEK and ABS. *Materials* **2015**, *8*, 5834–5846. [CrossRef]
27. Cicala, G.; Latteri, A.; Del Curto, B.; Lo Russo, A.; Recca, G.; Farè, S. Engineering Thermoplastics for Additive Manufacturing: A Critical Perspective with Experimental Evidence to Support Functional Applications. *J. Appl. Biomater. Funct. Mater.* **2017**, *15*, 10–18. [CrossRef]
28. Hu, B.; Xing, Z.; Wu, W.; Zhang, X.; Zhou, H.; Du, C.; Shan, B. Enhancing the Mechanical Properties of SCF/PEEK Composites in FDM via Process-Parameter Optimization. *High. Perform. Polym.* **2021**, *33*, 914–923. [CrossRef]
29. Zhen, H.; Zhao, B.; Quan, L.; Fu, J. Effect of 3D Printing Process Parameters and Heat Treatment Conditions on the Mechanical Properties and Microstructure of PEEK Parts. *Polymers* **2023**, *15*, 2209. [CrossRef]
30. Yang, C.; Tian, X.; Li, D.; Cao, Y.; Zhao, F.; Shi, C. Influence of Thermal Processing Conditions in 3D Printing on the Crystallinity and Mechanical Properties of PEEK Material. *J. Mater. Process. Technol.* **2017**, *248*, 1–7. [CrossRef]
31. Yang, D.; Cao, Y.; Zhang, Z.; Yin, Y.; Li, D. Effects of Crystallinity Control on Mechanical Properties of 3D-Printed Short-Carbon-Fiber-Reinforced Polyether Ether Ketone Composites. *Polym. Test.* **2021**, *97*, 107149. [CrossRef]
32. Rahman, K.M.; Letcher, T.; Reese, R. Mechanical Properties of Additively Manufactured PEEK Components Using Fused Filament Fabrication. In *Proceedings of the ASME 2015 International Mechanical Engineering Congress and Exposition*; Volume 2A: Advanced Manufacturing; American Society of Mechanical Engineers: New York, NY, USA, 2015. [CrossRef]
33. El Magri, A.; El Mabrouk, K.; Vaudreuil, S.; Chibane, H.; Touhami, M.E. Optimization of Printing Parameters for Improvement of Mechanical and Thermal Performances of 3D Printed Poly(Ether Ether Ketone) Parts. *J. Appl. Polym. Sci.* **2020**, *137*, 49087. [CrossRef]
34. Li, Y.; Lou, Y. Tensile and Bending Strength Improvements in PEEK Parts Using Fused Deposition Modelling 3D Printing Considering Multi-Factor Coupling. *Polymers* **2020**, *12*, 2497. [CrossRef]
35. Li, Y.; Han, X.; Ma, Z. Research on the Mechanical Properties of PEEK Material Artificial Bone Implants Fabricated by High-Temperature Air-Assisted 3D Printing. *J. Mech. Behav. Biomed. Mater.* **2026**, *173*, 107207. [CrossRef]
36. Sun, Q.; Shan, Z.; Zhan, L.; Wang, S.; Liu, X.; Li, Z.; Wu, S. Warp Deformation Model of Polyetheretherketone Composites Reinforced with Carbon Fibers in Additive Manufacturing. *Mater. Res. Express* **2021**, *8*, 125305. [CrossRef]
37. Lv, X.; Yang, S.; Pei, X.; Zhang, Y.; Wang, Q.; Wang, T. Enhanced Mechanical and Tribological Properties of 3D Printed Short Carbon Fiber Reinforced Polyether Ether Ketone Composites. *Polym. Compos.* **2024**, *45*, 8840–8860. [CrossRef]
38. Nyman, L.; Lehto, P.; Kukko, K.; Kestilä, A.; Kallio, E. Strength and Poisson's Ratio of Fused Filament Fabrication Parts Made from Carbon Filler Enhanced PEEK Compounds at Elevated Temperatures. *Sci. Rep.* **2024**, *14*, 31628. [CrossRef]
39. Stepanov, D.Y.; Dontsov, Y.V.; Panin, S.V.; Buslovich, D.G.; Alexenko, V.O.; Bochkareva, S.A.; Batranin, A.V.; Kosmachev, P.V. Optimization of 3D Printing Parameters of High Viscosity PEEK/30GF Composites. *Polymers* **2024**, *16*, 2601. [CrossRef]
40. Adarsh, S.H.; Nagamadhu, M. Effect of Printing Parameters on Mechanical Properties and Warpage of 3D-Printed PEEK/CF-PEEK Composites Using Multi-Objective Optimization Technique. *J. Compos. Sci.* **2025**, *9*, 208. [CrossRef]
41. Lu, S.; Zhang, B.; Wang, Y.; Bai, J.; Yang, C.; Sun, C.; Li, D. Sensitivity Analysis of Process Parameters on the Properties of Carbon Fiber Reinforced Polyether-Ether-Ketone Composites in Screw Extrusion 3D Printing. *Polym. Test.* **2025**, *150*, 108884. [CrossRef]
42. Puli, A.B.; Manjaiah, M.; Selvaraj, N.; Gokuldoss, P.K.; Joshi, A.G. Mechanical Response of FDM-Fabricated PEEK and Glass Fiber-Reinforced PEEK Under Varying Process Conditions. *J. Manuf. Mater. Process* **2026**, *10*, 110. [CrossRef]
43. Xu, S.; Yan, S.; Xie, X.; Zhang, X.; Qin, Y.; Li, Y.; Zheng, H. Predicting Failure Behaviour of Short Glass Fiber Reinforced PEEK Composites Using Anisotropic Elastoplastic Constitutive Model. *Polym. Compos.* **2026**, *47*, 16895–16909. [CrossRef]
44. Khosravani, M.R.; Berto, F.; Ayatollahi, M.R.; Reinicke, T. Fracture Behavior of Additively Manufactured Components: A Review. *Theor. Appl. Fract. Mech.* **2020**, *109*, 102763. [CrossRef]
45. Arif, M.F.; Kumar, S.; Varadarajan, K.M.; Cantwell, W.J. Performance of Biocompatible PEEK Processed by Fused Deposition Additive Manufacturing. *Mater. Des.* **2018**, *146*, 249–259. [CrossRef]
46. Yavas, D.; Zhang, Z.; Liu, Q.; Wu, D. Fracture Behavior of 3D Printed Carbon Fiber-Reinforced Polymer Composites. *Compos. Sci. Technol.* **2021**, *208*, 108741. [CrossRef]
47. Sharma, G.; Vuppuluri, A.; Udupa, A.; Suresh, K. Mixed-Mode I/II Fracture Investigation of 3D Printed Poly Ether Ether Ketone (PEEK). *Theor. Appl. Fract. Mech.* **2025**, *136*, 104854. [CrossRef]
48. Cicero, S.; Arrieta, S. Sensitivity to Notch Effect of Additively Manufactured Polymers and Polymer-Matrix Composites. *Procedia Struct. Integr.* **2026**, *77*, 56–63. [CrossRef]
49. Taylor, D. Predicting the Fracture Strength of Ceramic Materials Using the Theory of Critical Distances. *Eng. Fract. Mech.* **2004**, *71*, 2407–2416. [CrossRef]
50. Berto, F.; Lazzarin, P. Recent Developments in Brittle and Quasi-Brittle Failure Assessment of Engineering Materials by Means of Local Approaches. *Mater. Sci. Eng. R. Rep.* **2014**, *75*, 1–48. [CrossRef]

51. Taylor, D. *The Theory of Critical Distances*; Elsevier: Amsterdam, The Netherlands, 2007; ISBN 9780080444789. [CrossRef]
52. Whitney, J.M.; Nuismer, R.J. Stress Fracture Criteria for Laminated Composites Containing Stress Concentrations. *J. Compos. Mater.* **1974**, *8*, 253–265. [CrossRef]
53. Ibáñez-Gutiérrez, F.T.; Cicero, S.; Madrazo, V.; Berto, F. Fracture Loads Prediction on Notched Short Glass Fibre Reinforced Polyamide 6 Using the Strain Energy Density. *Phys. Mesomech.* **2018**, *21*, 165–172. [CrossRef]
54. Justo, J.; Castro, J. Mechanical Properties of 4 Rocks at Different Temperatures and Fracture Assessment Using the Strain Energy Density Criterion. *Geomech. Energy Environ.* **2021**, *25*, 100212. [CrossRef]
55. Sánchez, M.; Cicero, S.; Arrieta, S.; Torabi, A.R. Fracture Load Prediction of Non-Linear Structural Steels through Calibration of the ASED Criterion. *Metals* **2023**, *13*, 1211. [CrossRef]
56. Yang, M.; Yuan, W.; Dong, W.; Zhang, B.; Lu, Q. An Extended Average Strain Energy Density Criterion for Predicting Crack Propagation of Mixed Mode I-II Fracture in Concrete. *Eng. Fract. Mech.* **2025**, *321*, 111107. [CrossRef]
57. Seibert, P.; Susmel, L.; Berto, F.; Kästner, M.; Razavi, N. Applicability of Strain Energy Density Criterion for Fracture Prediction of Notched PLA Specimens Produced via Fused Deposition Modeling. *Eng. Fract. Mech.* **2021**, *258*, 108103. [CrossRef]
58. Ameri, B.; Taheri-Behrooz, F.; Aliha, M.R.M. Evaluation of the Geometrical Discontinuity Effect on Mixed-Mode I/II Fracture Load of FDM 3D-Printed Parts. *Theor. Appl. Fract. Mech.* **2021**, *113*, 102953. [CrossRef]
59. Sánchez, M.; Cicero, S.; Arrieta, S.; Martínez, V. Fracture Load Predictions in Additively Manufactured ABS U-Notched Specimens Using Average Strain Energy Density Criteria. *Materials* **2022**, *15*, 2372. [CrossRef]
60. Sánchez, M.; Arrieta, S.; Cicero, S. Fracture Load Estimations for U-Notched and V-Notched 3D Printed PLA and Graphene-Reinforced PLA Plates Using the ASED Criterion. *Frat. Ed. Integrità Strutt.* **2023**, *17*, 322–338. [CrossRef]
61. Cicero, S.; Arrieta, S. Fracture Load Predictions in 3D Printed Graphene-Reinforced PLA Notched Specimens Using the Average Strain Energy Density Criterion. In *Proceedings of the ASME 2023 Pressure Vessels and Piping Conference*; Volume 5: Materials & Fabrication; American Society of Mechanical Engineers: New York, NY, USA, 2023. [CrossRef]
62. Morettini, G.; Razavi, S.M.J.; Staffa, A.; Palmieri, M.; Berto, F.; Cianetti, F.; Braccesi, C. On the Combined Use of Averaged Strain Energy Density Criteria (ASED) and Equivalent Material Concept (ECC) for the Fracture Load Prediction of Additively Manufactured PLA v-Notched Specimens. *Procedia Struct. Integr.* **2023**, *47*, 296–309. [CrossRef]
63. Ghanbari, A.; Ayatollahi, M.R.; Choupani, N.; Torabi, A.R. Tensile Fracture of Blunt V-Notches in Rectangular Plates Additively Manufactured from Acrylonitrile Butadiene Styrene with Different Raster Angles. *Eng. Fail. Anal.* **2024**, *164*, 108670. [CrossRef]
64. Vălean, E.; Foti, P.; Berto, F.; Marșavina, L. Static and Fatigue Behavior of 3D Printed Smooth and Notched PLA and Short Carbon Fibers Reinforced PLA. *Theor. Appl. Fract. Mech.* **2024**, *131*, 104417. [CrossRef]
65. Majidi, H.R.; Nourani, A.; Farrahi, G.H. Fracture Prediction of Additively Manufactured PLA Notched Specimens Using Modified Energy-Based Failure Models. *Iran. J. Sci. Technol. Trans. Mech. Eng.* **2026**, *50*, 903–923. [CrossRef]
66. Naeimayi, M.; Choupani, N.; Ayatollahi, M.R.; Torabi, A.R. Blunt Notch Root Fracture Assessment in Additively Manufactured ABS Specimens with Symmetrical Cross-Ply Printing Configuration: Experiments versus Theories. *Theor. Appl. Fract. Mech.* **2026**, *145*, 105690. [CrossRef]
67. Peron, M.; Razavi, N.; Torgersen, J.; Berto, F. Fracture Assessment of PEEK under Static Loading by Means of the Local Strain Energy Density. *Materials* **2017**, *10*, 1423. [CrossRef]
68. Arrieta, S.; Cicero, S.; Sánchez, M.; Castanon-Jano, L. Estimation of Fracture Loads in 3D Printed PLA Notched Specimens Using the ASED Criterion. *Procedia Struct. Integr.* **2023**, *47*, 13–21. [CrossRef]
69. Sadeghian, H.; Ayatollahi, M.R.; Yazid Yahya, M. Effects of Copper Additives on Load Carrying Capacity and Micro Mechanisms of Fracture in 3D-Printed PLA Specimens. *Theor. Appl. Fract. Mech.* **2023**, *127*, 104027. [CrossRef]
70. Arrieta, S.; Cicero, S.; Álvarez, J.A. Prediction of Fracture Loads in 3D-Printed ASA and Carbon-Fiber Reinforced ASA Notched Specimens Using the Calibrated ASED Criterion. *Materials* **2025**, *18*, 4966. [CrossRef]
71. *ASTM D638-14*; Test Method for Tensile Properties of Plastics. ASTM International: West Conshohocken, PA, USA, 2014.
72. *ASTM D5045-14*; Test Methods for Plane-Strain Fracture Toughness and Strain Energy Release Rate of Plastic Materials. ASTM International: West Conshohocken, PA, USA, 2022.
73. Arrieta, S.; Cicero, S.; Munoz-Tymofyeyeva, D. Influence of Raster Orientations and Fiber Rinforcements on the Tensile Behavior and Fracture Toughnes of 3D-Printed PEEK. In *Proceedings of the ASME 2026 Pressure Vessels and Piping Conference*; Volume 5: Materials & Fabrication; American Society of Mechanical Engineers: New York, NY, USA, 2026. [CrossRef]
74. Sih, G.C. Strain-Energy-Density Factor Applied to Mixed Mode Crack Problems. *Int. J. Fract.* **1974**, *10*, 305–321. [CrossRef]
75. Lazzarin, P.; Zambardi, R. A Finite-Volume-Energy Based Approach to Predict the Static and Fatigue Behavior of Components with Sharp V-Shaped Notches. *Int. J. Fract.* **2001**, *112*, 275–298. [CrossRef]
76. Lazzarin, P.; Berto, F. Some Expressions for the Strain Energy in a Finite Volume Surrounding the Root of Blunt V-Notches. *Int. J. Fract.* **2005**, *135*, 161–185. [CrossRef]
77. Yosibash, Z.; Bussiba, A.; Gilad, I. Failure Criteria for Brittle Elastic Materials. *Int. J. Fract.* **2004**, *125*, 307–333. [CrossRef]
78. Seweryn, A. Brittle Fracture Criterion for Structures with Sharp Notches. *Eng. Fract. Mech.* **1994**, *47*, 673–681. [CrossRef]

79. Berto, F.; Lazzarin, P. A Review of the Volume-Based Strain Energy Density Approach Applied to V-Notches and Welded Structures. *Theor. Appl. Fract. Mech.* **2009**, *52*, 183–194. [CrossRef]
80. Arif, M.F.; Alhashmi, H.; Varadarajan, K.M.; Koo, J.H.; Hart, A.J.; Kumar, S. Multifunctional Performance of Carbon Nanotubes and Graphene Nanoplatelets Reinforced PEEK Composites Enabled via FFF Additive Manufacturing. *Compos. Part B Eng.* **2020**, *184*, 107625. [CrossRef]
81. *ANSYS ANSYS Mechanical*, version 2023 R1; ANSYS, Inc.: Canonsburg, PA, USA, 2023.
82. Seibert, P.; Taylor, D.; Berto, F.; Mohammad Javad Razavi, S.; Razavi, N. Energy TCD—Robust and Simple Failure Prediction Unifying the TCD and ASED Criterion. *Eng. Fract. Mech.* **2022**, *271*, 108652. [CrossRef]
83. Al Helal, M.; Almutairi, A.; Almudayris, S.; Ali, U.; Albinmousa, J. Estimation of Mode I Quasi-Static Fracture of Notched Aluminum–Lithium AW2099-T83 Alloy Using Local Approaches and Machine Learning. *Eng. Fail. Anal.* **2024**, *163*, 108496. [CrossRef]
84. Arrieta, S.; Cicero, S.; Muñoz-Tymofyeyeva, D. *Notch Effect in Polyetheretherketone (PEEK): Tensile and Fracture Tests—FRADDCO Project*; Zenodo: Geneva, Switzerland, 2026. [CrossRef]
85. Arrieta, S.; Cicero, S.; Muñoz-Tymofyeyeva, D. *Notch Effect in Carbon Fiber Reinforced Polyetheretherketone (PEEK-CF): Tensile and Fracture Tests—FRADDCO Project*; Zenodo: Geneva, Switzerland, 2026. [CrossRef]
86. Arrieta, S.; Cicero, S.; Muñoz-Tymofyeyeva, D. *Notch Effect in Glass Fiber Reinforced Polyetheretherketone (PEEK-GF): Tensile and Fracture Tests—FRADDCO Project*; Zenodo: Geneva, Switzerland, 2026. [CrossRef]

Disclaimer/Publisher's Note: The statements, opinions and data contained in all publications are solely those of the individual author(s) and contributor(s) and not of MDPI and/or the editor(s). MDPI and/or the editor(s) disclaim responsibility for any injury to people or property resulting from any ideas, methods, instructions or products referred to in the content.